AD-A137 353 NUMERICAL SOLUTIONS TO ILL-POSED AND WELL-POSED IMPEDANCE BOUNDARY CONDIT..(U) MASSACHUSETTS INST OF TECH LEXINGTON LINCOLN LAB J R ROGERS 30 NOV 83 TR-641 1/2

UNCLASSIFIED ESD-TR-83-106 F19628-80-C-0002 F/G 12/1 NL

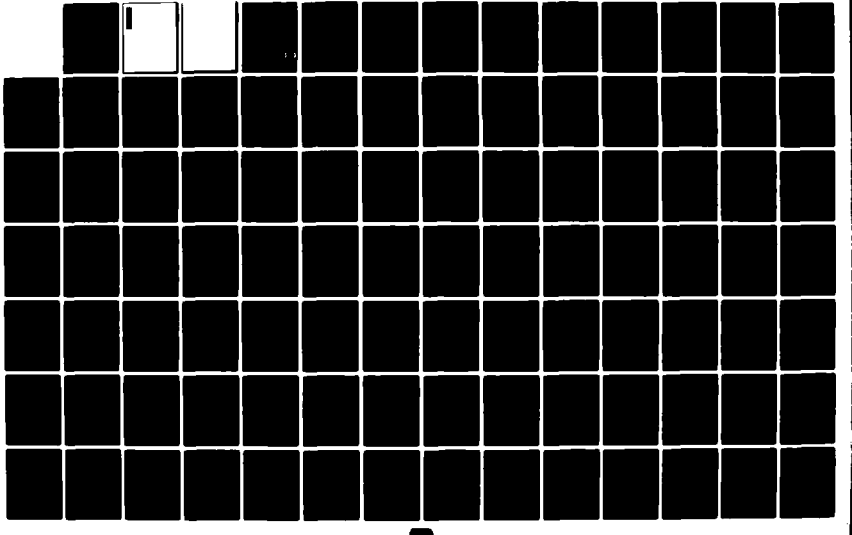

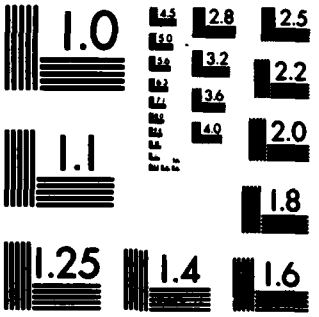

MICROCOPY RESOLUTION TEST CHART
NATIONAL BUREAU OF STANDARDS-1963-A

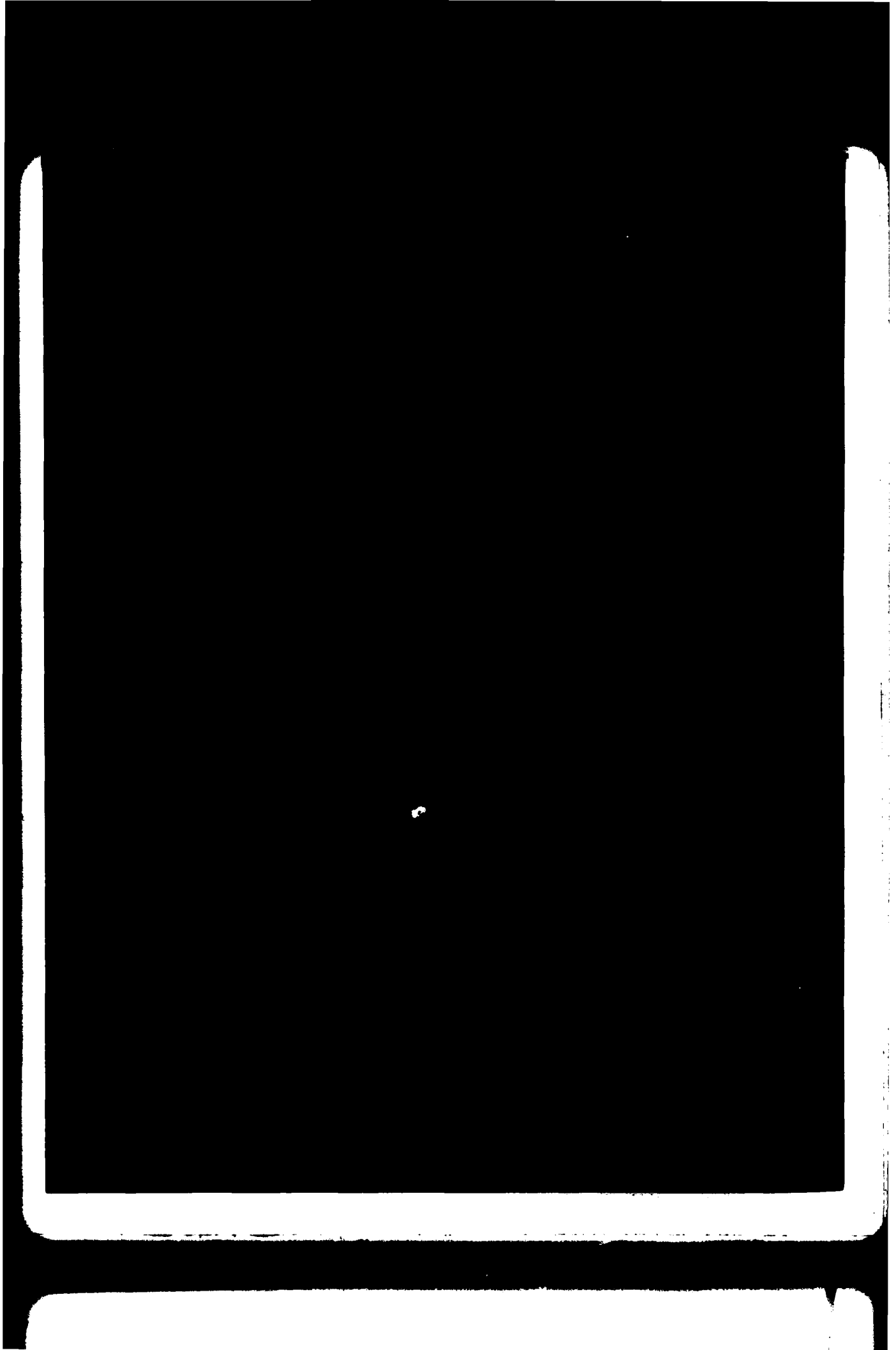

MASSACHUSETTS INSTITUTE OF TECHNOLOGY
LINCOLN LABORATORY

NUMERICAL SOLUTIONS TO ILL-POSED AND WELL-POSED IMPEDANCE BOUNDARY CONDITION INTEGRAL EQUATIONS

J.R. ROGERS

Group 34

TECHNICAL REPORT 641

30 NOVEMBER 1983

LEXINGTON MASSACHUSETTS

ABSTRACT

Exterior scattering from a three-dimensional impedance body can be formulated in terms of various integral equations derived from the Leontovich impedance boundary condition (IBC). The electric and magnetic field integral equations are ill-posed because they theoretically admit spurious solutions at the frequencies of interior perfect conductor cavity resonances. A combined field formulation is well-posed because it does not allow the spurious solutions. This report outlines the derivation of IBC integral equations and describes a procedure for constructing moment-method solutions for bodies of revolution. Numerical results for scattering from impedance spheres are presented which contrast the stability and accuracy of solutions to the ill-posed equations with those of the well-posed equation. The results show that numerical solutions for exterior scattering to the electric and magnetic field integral equations can be severely contaminated by spurious resonant solutions regardless of whether the surface impedance of the body is lossy or lossless. Solutions to the combined field equation are not contaminated by the spurious solutions when a suitable choice of integral equation weighting coefficient can be determined. However, the determination of the weighting coefficient for the general impedance case is more difficult and more critical than for the perfectly conducting scatterer case.

CONTENTS

1. INTRODUCTION

A well-known method for modeling electromagnetic interactions with certain types of imperfectly conducting bodies involves describing the body surface with a Leontovich impedance boundary condition (IBC).[1-4] This approximation makes integral equation formulations of scattering problems nearly as simple as those for perfectly conducting bodies.[5] Until the present, solutions to IBC integral equations for exterior scattering from generally-shaped, three-dimensional bodies have been obtained from either the magnetic field integral equation (MFIE)[6-8] or the electric field integral equation (EFIE).[9] These two IBC equations can be described as being mathematically ill-posed for exterior scattering problems because at certain discrete frequencies, the integral operators of each become singular and the equations no longer have unique solutions.[10] These discrete frequencies are the interior resonances of a perfectly conducting cavity having the same shape as the impedance target.[10] Numerical solutions to either the MFIE or EFIE near a cavity resonance will result in ill-conditioned matrices and scattering results which may be contaminated by spurious solutions due to the cavity resonances.* In contrast to the MFIE and EFIE, the

---

* The terminology "spurious solutions" refers to unwanted mathematical solutions which have no physical connection with the exterior scattering problem.

IBC combined field integral equation (CFIE) is mathematically well-posed because it does not allow the spurious resonant solutions.[10]

This report investigates numerical solutions for scattering from an impedance body of revolution (BOR) as determined by the MFIE, EFIE and the CFIE. The principal objectives are to: (1) describe the method by which moment-method solutions to the three equations can be constructed, (2) contrast the numerical stability and accuracy of solutions to the MFIE and the EFIE with those of the CFIE, and (3) investigate the sensitivity of the CFIE to parameters such as integral equation weighting coefficient and moment-method segmentation for various types of surface impedance (i.e. reactive, lossy, etc.). The report begins with a brief discussion in Section 2 of the derivation of the three equations and the well-posedness of each.* In Section 3 it will be described how existing moment-method numerical algorithms applicable to scattering from perfectly conducting BORs[11-13] can easily be generalized to the IBC case. A Fortran IV computer program which contains the modifications discussed in Section 3 is listed in Appendix A. Numerical results which address objectives (2) and (3) above are

---

* A general, theoretical treatment of the well-posedness of IBC integral equations is given in Ref. 10. The numerical results of this report represent the practical implementation of one of the methods discussed in Ref. 10.

presented in Section 4. These results are for scattering from impedance spheres, and in all cases the moment-method solutions were compared to an "exact" series solution.[14]

Some conclusions concerning the results are presented in Section 5. Briefly, the results demonstrate that numerical solutions to the MFIE and EFIE for exterior scattering can be severely contaminated by spurious solutions regardless of whether the surface impedance is lossy or lossless. The errors in predicting scattering from bodies having non-zero surface impedances are, in general, larger than for the perfectly conducting case.* Also, the results demonstrate that the solution accuracy of the CFIE as a function of integral equation weighting coefficient and moment-method segmentation is strongly influenced by the value of surface impedance. Criteria established for the perfect perfect conductor case[7,11] may not work well when the surface impedance is non-zero.

---

* A perfectly conducting surface can be considered as the special case of an impedance surface when the surface impedance equals zero.

2.0 REVIEW OF THE FORMULATION AND STABILITY OF IMPEDANCE BOUNDARY CONDITION INTEGRAL EQUATIONS

The physical scattering problem is depicted in Fig. 2.1. A uniform plane electromagnetic wave $(\hat{E}^i, \hat{H}^i)$* is incident upon an imperfectly conducting body surrounded by a closed surface S. $(\hat{E}^i, \hat{H}^i)$ are assumed known and have a monochromatic time variation of $e^{j\omega t}$. When the incident wave interacts with the body, volume electric current density, $\hat{J}_{vol}$, is induced inside S and radiates a scattered field $(\hat{E}^s, \hat{H}^s)$. Assuming that the radiation conditions are met and the target is passive, the scattered fields are unique.

In solving the problem depicted in Fig. 2.1, it is often useful to apply the Equivalence Principle[15] which states that the body with volume electric currents can be conceptually replaced by a sourceless volume having electric $(\hat{J})$ and magnetic $(\hat{M})$ surface current densities on S. The jump conditions which must be satisfied on S are:[15]

$$\hat{n} \times (\hat{E}_+ - \hat{E}_-) = - \hat{M} \tag{2.1}$$

$$\hat{n} \times (\hat{H}_+ - \hat{H}_-) = \hat{J} \tag{2.2}$$

---

* The field point dependence $(\hat{r})$ of all vectors and dyadics is suppressed in most cases throughout the text.

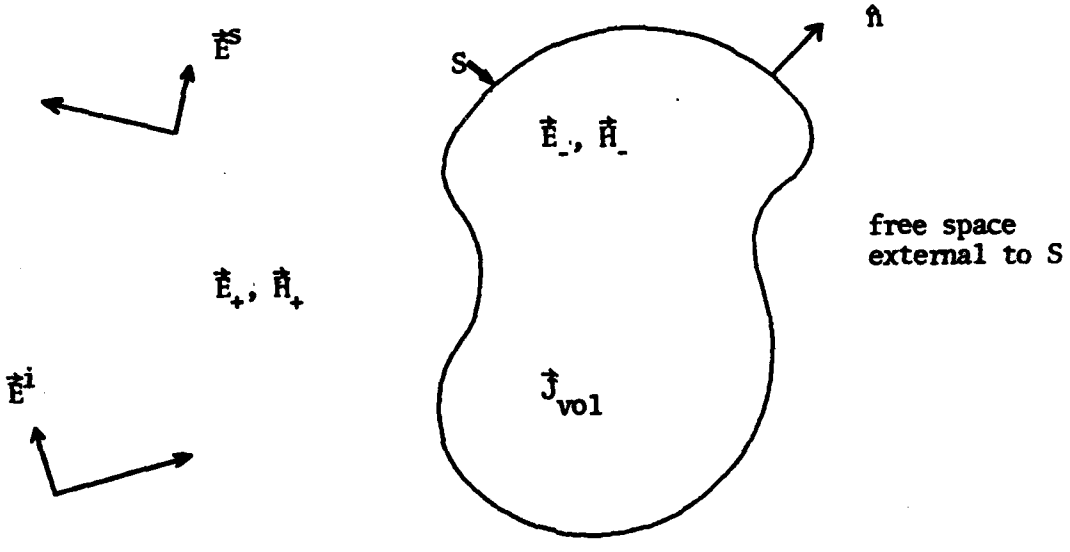

Fig. 2.1. Generalized problem for scattering from an imperfectly conducting body.

where $(\hat{E}_{\pm},\hat{H}_{\pm})$ are the total electric and magnetic fields just outside (+) or just inside (-) the surface and $\hat{n}$ is the outward unit normal to the surface. These total fields are the sums of incident fields due to sources at infinity and scattered fields due to $(\hat{J},\hat{M})$:

$$\hat{E}_{\pm} = \hat{E}^{i} + \hat{E}^{s}_{\pm} \tag{2.3}$$

$$\hat{H}_{\pm} = \hat{H}^{i} + \hat{H}^{s}_{\pm} \tag{2.4}$$

In constructing appropriate integral equations, a certain arbitrariness exists in the choices of $(\hat{J},\hat{M})$ and $(\hat{E}_{-},\hat{H}_{-})$. Although the exterior fields must be unique, there are infinitely many sets of equivalent currents and interior fields which will give rise to the correct exterior fields. Thus, one can choose $(\hat{E}_{-},\hat{H}_{-})$ when formulating the problem in order to obtain unique equivalent currents. As depicted in Fig. 2.2, a convenient choice for the interior fields is often the null field.

Assume that an imperfectly conducting body has the following Leontovich impedance boundary condition (IBC) satisfied on its surface[1-4]:

$$\hat{n} \times \hat{E}_{+} \times \hat{n} = \eta \, \bar{\bar{Z}}_{s} \cdot (\hat{n} \times \hat{H}_{+}) \tag{2.5}$$

where $\bar{\bar{Z}}_{s}$ is the normalized dyadic surface impedance of the body containing information about the material properties within S and

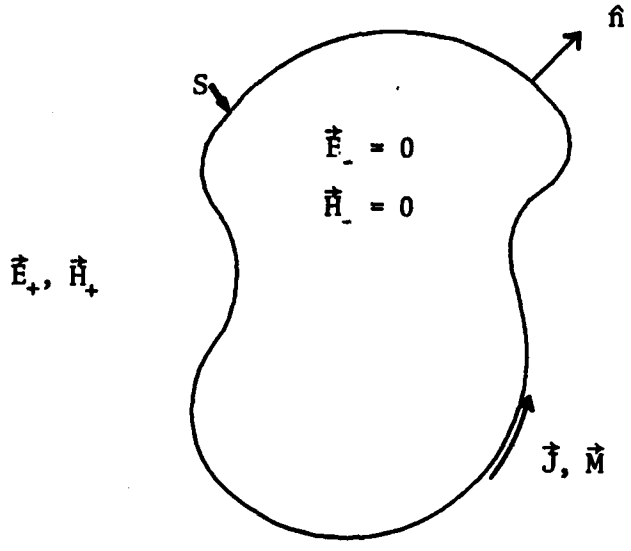

Fig. 2.2. Null interior field equivalent problem.

η is the free space wave impedance. Upon substitution of Eqs. 2.1 and 2.2 into Eq. 2.5, the following condition relating the tangential components of the interior fields to the equivalent currents is obtained:

$$\hat{E}_- \times \hat{n} + \hat{M} =$$

$$-\eta\, \hat{n} \times \bar{\bar{Z}}_s \cdot \hat{J} - \eta\, \hat{n} \times \bar{\bar{Z}}_s \cdot (\hat{n} \times \hat{H}_-) \qquad (2.6)$$

When choosing the null field problem depicted in Fig. 2.2, the following two conditions must hold on the surface:

$$\hat{n} \times \hat{E}_- = 0 \qquad (2.7)$$

$$\hat{n} \times \hat{H}_- = 0 \qquad (2.8)$$

For this choice of $(\hat{E}_-, \hat{H}_-)$ a simple relationship for $\hat{M}$ in terms of $\hat{J}$ is obtained:

$$\hat{M} = -\eta\, \hat{n} \times \bar{\bar{Z}}_s \cdot \hat{J} \qquad (2.9)$$

This last relation effectively reduces the problem from two coupled vector integral equations in two vector unknowns, $(\hat{J}, \hat{M})$, to one vector integral equation in one vector unknown, $\hat{J}$. Note that each vector integral equation consists of two coupled scalar integral equations in two scalar unknowns. Equations 2.7 and 2.8

each lead to a different vector integral equation for the unique source $\underline{J}$. Using equations 2.3 and 2.4 and integral representations for $\underline{E}^s$ and $\underline{H}^s$ in terms of $(\underline{J},\underline{M})$,[15,16] Eqs. 2.7 and 2.8 lead to the following IBC electric field integral equation (EFIE) and IBC magnetic field integral equation (MFIE), respectively:

$$\hat{n} \times \underline{E}^i = -\frac{\underline{M}}{2} + \hat{n} \times \int_s [j\omega\mu \underline{J}(\underline{r}') \phi + \underline{M}(\underline{r}') \times \nabla'\phi + \frac{1}{j\omega\epsilon} \nabla'\cdot\underline{J}(\underline{r}') \nabla'\phi] ds' \qquad \text{EFIE (2.10)}$$

$$\hat{n} \times \underline{H}^i = \frac{\underline{J}}{2} - \hat{n} \times \int_s [-j\omega\epsilon \underline{M}(\underline{r}') \phi + \underline{J}(\underline{r}') \times \nabla'\phi - \frac{1}{j\omega\mu} \nabla'\cdot \underline{M}(\underline{r}') \nabla'\phi] ds' \qquad \text{MFIE (2.11)}$$

where

$$\underline{M} = -\eta\, \hat{n} \times \underline{\underline{Z}}_s \cdot \underline{J}$$

and

$$\phi = \frac{1}{4\pi} \frac{e^{-jk\left|\underline{r}-\underline{r}'\right|}}{\left|\underline{r}-\underline{r}'\right|}$$

Equations 2.10 and 2.11 are valid in the limit as $\underline{r} \to S$ from the inside. The terminology "EFIE" and "MFIE" in this report will denote the generalized impedance electric and magnetic field

integral equations. The perfect conductor equations are the special cases when $Z_s \equiv 0$.

By the choice of vanishing interior fields, two different vector integral equations were obtained for determining a unique source $\bar{J}$. Although it would appear that either the EFIE or MFIE could be solved for $\bar{J}$, the solution must ensure that both equations are satisfied. This is required because Eq. 2.9 (used in the solution for $\bar{J}$) is valid only if both Eqs. 2.7 and 2.8 are satisfied. Here-to-fore, it has been assumed that a solution to either the MFIE or the EFIE will satisfy both equations. However, that assumption is valid only away from discrete frequencies located at the perfect conductor (p.c.) interior cavity resonant frequencies.[10] At a p.c. cavity resonant frequency, the right hand sides of both Eqs. 2.10 and 2.11 are singular allowing non-unique mathematical solutions to exist at that frequency.[10] Consequently, sets of spurious equivalent currents which are solutions to the homogeneous perfect conductor equations can contaminate the particular scattering solution. Thus, Eqs. 2.10 and 2.11 are not equivalent to each other at a p.c. cavity resonant frequency and the solution technique must ensure that both are satisfied.

Although uniqueness problems with the EFIE and the MFIE occur at discrete frequencies, it is still advantageous to have an integral equation formulation which ensures a unique solution at all frequencies. This is due to the fact that numerical

solutions to either ill-posed equation will be contaminated within some bandwidth about a spurious resonance (due to the approximation of an integral equation with a matrix equation, numerical roundoff error, etc.). Since the perfect conductor cavity resonances of a generally-shaped target are not known a priori and become increasingly closely spaced with increasing frequency, it is apparent that for large scattering targets (with respect to a wavelength) the EFIE and the MFIE may be unreliable at all frequencies.

If Eqs. 2.7 and 2.8 lead to two equations for a unique source $\vec{J}$, then a linear combination will also yield a solution:

$$\hat{n} \times \vec{E}_- + Z_a \cdot \hat{n} \times \vec{H}_- = 0 \qquad (2.12)$$

where Z_a is some arbitrary, generalized weighting coefficient which could be a function of $\vec{r}$. When substituting Eqs. 2.3 and 2.4 into 2.12, along with the appropriate integral representations for $\vec{E}^s$ and $\vec{H}^s$, one obtains an IBC combined field integral equation (CFIE). It can be shown that a solution to the CFIE will ensure that both 2.7 and 2.8 are satisfied at all frequencies when Z_a is not reactive.[10] Thus, the CFIE for the impedance body case rejects spurious resonances in a similar fashion as does the perfect conductor CFIE.[11,12]

3.0 GENERALIZATION OF PERFECT CONDUCTOR MOMENT-METHOD ALGORITHMS TO THE IMPEDANCE BODY CASE

3.1 IBC Integral Equations in Perfect Conductor Integral Operator Form

In Section 2, three impedance boundary condition integral equations were derived and the well-posedness of each was briefly discussed. The EFIE and MFIE formulations are ill-posed due to non-uniqueness at interior resonant frequencies of the perfectly conducting cavity. The CFIE, on the other hand, is well-posed at all frequencies (provided $\tilde{Z}_a$ is non-reactive). In this section, it will be shown how numerical solutions to each of these equations can be constructed from moment-method matrix operators applicable to scattering from a perfectly conducting body. A main computer program which accomplishes this procedure for bodies of revolution is listed in Appendix A.

The particular perfect conductor algorithms to be generalized are those of Mautz and Harrington.[12,13] These moment-method programs were chosen because of their wide availability and good documentation, and because they contain all the required matrix operators for solving the IBC equations. Although the programs are restricted to bodies of revolution, the basic procedure in extending these programs to the impedance body case would also be applicable to moment-method programs for more generally-shaped bodies. It should be noted that the procedure

to be described in this section has already been accomplished for the EFIE by Iskander, et. al.[9]*

It is appropriate to first recast the IBC integral equations into operator notation applicable to Mautz and Harrington's equations. Their integral equations for scattering from a perfectly conducting body can be written as:[11,12]

$$\frac{1}{\eta}\,\hat{n} \times \vec{E}^{i} \times \hat{n} = L_E(\vec{J}) \tag{3.1}$$

$$\hat{n} \times \vec{H}^{i} = L_H(\vec{J}) \tag{3.2}$$

where the integral representations of the operators L_E and L_H are:

$$L_E(\vec{J}) = \frac{-1}{\eta}\,\hat{n} \times \hat{n} \times \int_s \left[j\omega\mu\, \vec{J}(\vec{r}')\,\phi + \frac{1}{j\omega\varepsilon}\,\nabla'\cdot\vec{J}(\vec{r}')\,\nabla'\phi\right] ds' \tag{3.3}$$

$$L_H(\vec{J}) = \frac{\vec{J}}{2} - \hat{n} \times \int_s \vec{J}(r') \times \nabla'\phi\, ds' \tag{3.4}$$

Equations 3.1 and 3.2 are the perfect conductor special cases of the IBC EFIE and MFIE equations with the EFIE put into similar vector direction and units as that of the MFIE.

In terms of the perfect conductor operators, L_E and L_H, the IBC integral equations are:

---

* The formulas in Ref. 9 should be used with caution. In addition to the dyadic impedance boundary condition definition being unclear, there appears to be a minus sign error in that definition which is carried throughout all subsequent equations.

$$\frac{1}{\eta}\,\hat{n} \times \vec{E}^i \times \hat{n} = L_E(\vec{J}) + \hat{n} \times L_H(\frac{\vec{M}}{\eta}) \qquad \text{EFIE} \quad (3.5)$$

$$\hat{n} \times \vec{H}^i = L_H(\vec{J}) + \hat{n} \times L_E(\frac{\vec{M}}{\eta}) \qquad \text{MFIE} \quad (3.6)$$

$$\hat{n} \times \vec{H}^i + \alpha\,\frac{1}{\eta}\,\hat{n} \times \vec{E}^i \times \hat{n} = L_H(\vec{J}) + \alpha\, L_E(\vec{J})$$

$$+ \hat{n} \times L_E(\frac{\vec{M}}{\eta}) + \alpha\,\hat{n} \times L_H(\frac{\vec{M}}{\eta}) \qquad \text{CFIE} \quad (3.7)$$

where α is a constant coefficient in the CFIE.

3.2 Review of the Moment-Method Solution for Scattering from a Perfectly Conducting Body

Mautz and Harrington[11-13] solve Eqs. 3.1 and 3.2 for a body of revolution (BOR) using the geometry in Fig. 3.1. The coordinates $(\hat{n},\hat{\phi},\hat{t})$ represent a right-handed, orthogonal system for describing vectors on the BOR surface. The unknown electric surface current density, consisting of $\hat{t}$ and $\hat{\phi}$ components, is expanded in terms of a Fourier series in ϕ and in terms of overlapping triangular expansion functions, f, in t:

$$\vec{J}(\vec{r}) = J^t(t,\phi)\,\hat{t} + J^\phi(t,\phi)\,\hat{\phi}$$

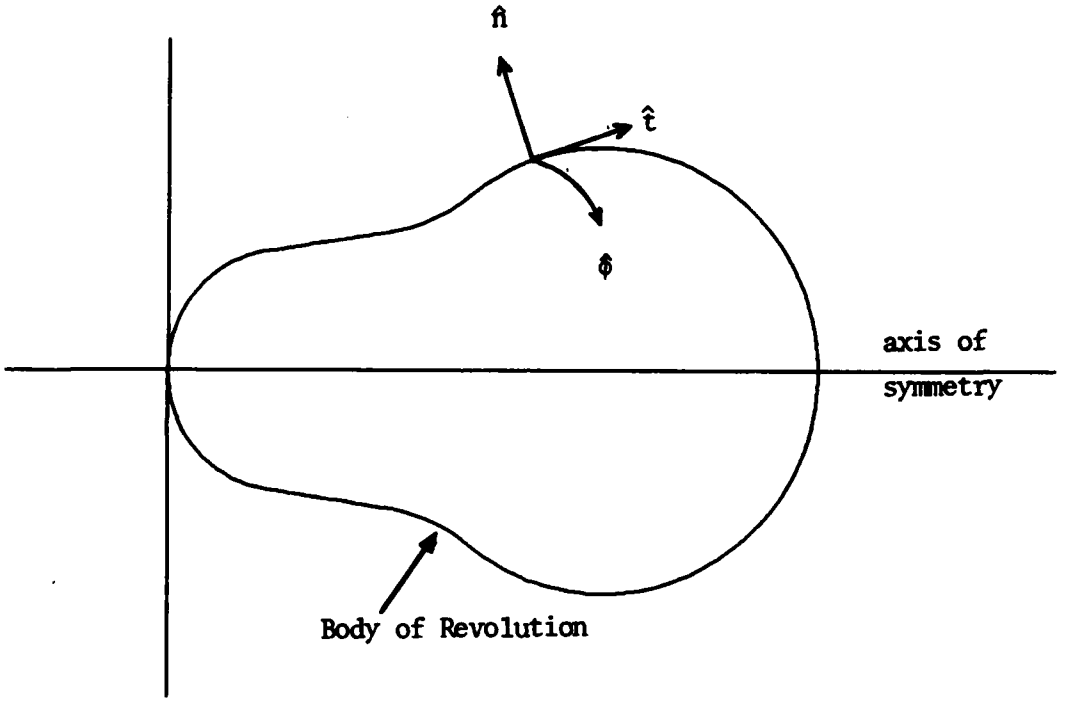

Fig. 3.1. Right-handed, orthogonal, curvilinear coordinate system ($\hat{n}$, $\hat{\phi}$, $\hat{t}$) on the surface of a body of revolution.

where,

$$J^t(t,\phi) = \sum_{n=1}^{N} \sum_{k=1}^{K} I^t_{nk} f_k(t) e^{jn\phi}$$
$$J^\phi(t,\phi) = \sum_{n=1}^{N} \sum_{k=1}^{K} I^\phi_{nk} f_k(t) e^{jn\phi} \qquad (3.8)$$

To determine the number and location of all $f_k(t)$, the top half of the BOR profile is segmented into short straight line segments. The number of expansion functions, K, is approximately 1/2 the number of straight line segments. For a visual description of the triangle functions see Ref. 12.

Mautz and Harrington define vector testing functions, $\hat{W}$, as:

$$\hat{W}(\vec{r}) = W^t(t,\phi)\ \hat{t} + W^\phi(t,\phi)\ \hat{\phi}$$

where

$$W^t(t,\phi) = W^\phi(t,\phi) = \sum_{m=1}^{N} \sum_{i=1}^{K} f_i(t) e^{-jm\phi} \qquad (3.9)$$

Upon substitution of the expansion for $\hat{J}$ into Eqs. 3.1 and 3.2 and taking the appropriate inner products of the equations with the testing functions, one obtains a series of independent matrix equations corresponding to the various Fourier modes. (The Fourier series inner product is non-zero only for m=n due to the azimuthal symmetry of the problem.) For the n^{th} Fourier mode:

$$[V_n] = [Z_n]\,[I_n] \tag{3.10}$$

$$[U_n] = [Y_n]\,[I_n] \tag{3.11}$$

or, expressing the vector nature of the equations:

$$\begin{bmatrix} V_n^t \\ V_n^\phi \end{bmatrix} = \begin{bmatrix} Z_n^{tt} & Z_n^{t\phi} \\ Z_n^{\phi t} & Z_n^{\phi\phi} \end{bmatrix} \begin{bmatrix} I_n^t \\ I_n^\phi \end{bmatrix} \tag{3.12}$$

$$\begin{bmatrix} U_n^t \\ U_n^\phi \end{bmatrix} = \begin{bmatrix} Y_n^{tt} & Y_n^{t\phi} \\ Y_n^{\phi t} & Y_n^{\phi\phi} \end{bmatrix} \begin{bmatrix} I_n^t \\ I_n^\phi \end{bmatrix} \tag{3.13}$$

Equations 3.10 and 3.11 are the n^{th} mode matrix representations of Eqs. 3.1 and 3.2 respectively. The known vectors, $[V_n]$ and $[U_n]$, each contain 2K elements which are obtained from the inner products of the incident fields with the testing functions. The vector $[I_n]$ contains the 2K unknown expansion coefficients for the n^{th} Fourier mode of $\vec{J}$. $[Z_n]$ and $[Y_n]$ are 2K x 2K square matrices and can be interpreted as normalized impedance and admittance matrices (not to be confused with surface impedance or admittance). Explicit expressions for the elements of $[V_n]$, $[U_n]$, $[Z_n]$ and $[Y_n]$ are given in Ref. 12. For

each Fourier mode retained in the solution, equation 3.10 or 3.11 (or Mautz and Harrington's perfect conductor combined field equation) can be solved for the $[I_n]$ by using matrix inversion or factorization. The scattered field due to the equivalent currents of each mode can then be calculated and summed up for the total scattering solution.

3.3 Generalizing the Moment-Method Solution to the Impedance Body Case

For the IBC case, the appropriate integral equations are given in operator form in Eqs. 3.5, 3.6 and 3.7. These integral equations were derived from the impedance boundary condition of Eq. 2.5 assuming vanishing interior fields. The derivations led to an expression for $\bar{M}$ in terms of $\bar{J}$, restated here for convenience:

$$\bar{M} = -\eta\, \hat{n} \times \bar{\bar{Z}}_s \cdot \bar{J} \tag{2.9}$$

Assume that the normalized dyadic surface impedance is diagonal and only a slowly varying function of t:

$$\bar{\bar{Z}}_s(\bar{r}) = Z_s^t(t)\, \hat{t}\hat{t} + Z_s^\phi(t)\, \hat{\phi}\hat{\phi} \tag{3.14}$$

$\bar{\bar{Z}}_s$ will be discretized over the coordinate t but will be assumed to be approximately constant over any particular segment.

In applying the moment-method for the IBC case, let $\hat{M}$ be expanded similar to $\hat{J}$:

$$M^t(t,\phi) = \sum_{n=1}^{N} \sum_{k=1}^{K} M_{nk}^t \, f_k(t) \, e^{jn\phi}$$

$$M^\phi(t,\phi) = \sum_{n=1}^{N} \sum_{k=1}^{K} M_{nk}^\phi \, f_k(t) \, e^{jn\phi} \qquad (3.15)$$

Using equations 2.9 and 3.12, the elements of $[M_n]$ can be expressed in terms of the $[I_n]$ as:

$$M_{nk}^t = -\eta \, (Z_s^\phi)_k \, I_{nk}^\phi$$

$$M_{nk}^\phi = \eta \, (Z_s^t)_k \, I_{nk}^t \qquad (3.16)$$

Substitute the expansions for $\hat{J}$ and $\hat{M}$, equations 3.8 and 3.15, into each IBC integral equation and take the appropriate inner products with the testing functions. For the n^{th} Fourier mode, Eqs. 3.5 and 3.6 can be expressed in matrix form respectively as:

$$[V_n] = [Z_n]\,[I_n] + \frac{1}{\eta}\,[N]\,[Y_n]\,[M_n] \tag{3.17}$$

$$[U_n] = [Y_n]\,[I_n] + \frac{1}{\eta}\,[N]\,[Z_n]\,[M_n] \tag{3.18}$$

The matrix [N] represents the $\hat{n}$ x vector operation and can be expressed as:

$$[N] = \begin{bmatrix} 0 & I \\ -I & 0 \end{bmatrix} \tag{3.19}$$

where the K x K submatrix I is the identity matrix. It is desired to convert Eqs. 3.17 and 3.18 into the following forms respectively:

$$[V_n] = [ZZ_n]\,[I_n] \tag{3.20}$$

$$[U_n] = [YY_n]\,[I_n] \tag{3.21}$$

where $[ZZ_n]$ and $[YY_n]$ can be thought of as the generalized, normalized impedance and admittance matrices for the IBC equations. In each of Eqs. 3.17 and 3.18, there is a term of the form $\frac{1}{\eta}\,[N]\,[A_n]\,[M_n]$ which must be converted into the form $[B_n][I_n]$. This is accomplished by the following steps. Applying the $\hat{n}$ x operation:

$$\frac{1}{\eta}\,[N]\,[A_n]\,[M_n] \;=\; \frac{1}{\eta}\begin{bmatrix} A_n^{\phi t} & A_n^{\phi\phi} \\ -A_n^{tt} & -A_n^{t\phi} \end{bmatrix}\begin{bmatrix} M_n^{t} \\ M_n^{\phi} \end{bmatrix} \qquad (3.22)$$

using Eq. 3.14:

$$\frac{1}{\eta}\,[N]\,[A_n]\,[M_n] \;=\; \begin{bmatrix} A_n^{\phi t} & A_n^{\phi\phi} \\ -A_n^{tt} & -A_n^{t\phi} \end{bmatrix}\begin{bmatrix} -Z_s^{\phi} & I_n^{\phi} \\ Z_s^{t} & I_n^{t} \end{bmatrix} \qquad (3.23)$$

Reordering the matrix equation to obtain the electric current expansion coefficients in their proper order:

$$\frac{1}{\eta}\,[N]\,[A_n]\,[M_n] \;=\; \begin{bmatrix} A_n^{\phi\phi} & -A_n^{\phi t} \\ -A_n^{t\phi} & A_n^{tt} \end{bmatrix}\begin{bmatrix} Z_s^{t} & I_n^{t} \\ Z_s^{\phi} & I_n^{\phi} \end{bmatrix} \qquad (3.24)$$

Then, under the assumption that the discretized form of $\bar{\bar{Z}}_s$ has individual elements which are constant with respect to t:

$$\frac{1}{\eta}\,[N]\,[A_n]\,[M_n] = [B_n][I_n]$$

where the elements of $[B_n]$ are given by: (i=row, j=column)

$$
\begin{aligned}
(B_n^{tt})_{ij} &= (A_n^{\phi\phi})_{ij}\ (Z_s^t)_j \\
(B_n^{t\phi})_{ij} &= -(A_n^{\phi t})_{ij}\ (Z_s^\phi)_j \\
(B_n^{\phi t})_{ij} &= -(A_n^{t\phi})_{ij}\ (Z_s^t)_j \\
(B_n^{\phi\phi})_{ij} &= (A_n^{tt})_{ij}\ (Z_s^\phi)_j
\end{aligned}
\qquad (3.25)
$$

The matrix elements appropriate to each IBC equation can now be written down by inspection (in terms of the matrices pertaining to the perfect conductor equations). For the n^{th} Fourier mode, the matrix representations of Eqs. 3.5, 3.6 and 3.7 are:

$$
\begin{bmatrix} V_n^t \\ V_n^\phi \end{bmatrix} = \begin{bmatrix} ZZ_n^{tt} & ZZ_n^{t\phi} \\ ZZ_n^{\phi t} & ZZ_n^{\phi\phi} \end{bmatrix} \begin{bmatrix} I_n^t \\ I_n^\phi \end{bmatrix} \qquad \text{EFIE (3.26)}
$$

$$
\begin{bmatrix} U_n^t \\ U_n^\phi \end{bmatrix} = \begin{bmatrix} YY_n^{tt} & YY_n^{t\phi} \\ YY_n^{\phi t} & YY_n^{\phi\phi} \end{bmatrix} \begin{bmatrix} I_n^t \\ I_n^\phi \end{bmatrix} \qquad \text{MFIE (3.27)}
$$

$$
\begin{bmatrix} U_n^t+\alpha V_n^t \\ U_n^\phi+\alpha V_n^\phi \end{bmatrix} = \begin{bmatrix} YY_n^{tt}+\alpha ZZ_n^{tt} & YY_n^{t\phi}+\alpha ZZ_n^{t\phi} \\ YY_n^{\phi t}+\alpha ZZ_n^{\phi t} & YY_n^{\phi\phi}+\alpha ZZ_n^{\phi\phi} \end{bmatrix} \begin{bmatrix} I_n^t \\ I_n^\phi \end{bmatrix} \qquad \text{CFIE (3.28)}
$$

where the elements of $[ZZ_n]$ are given by: (i=row, j=column)

$$
\begin{aligned}
(ZZ_n^{tt})_{ij} &= (Z_n^{tt})_{ij} + (Z_s^{t})_j \, (Y_n^{\phi\phi})_{ij} \\
(ZZ_n^{t\phi})_{ij} &= (Z_n^{t\phi})_{ij} - (Z_s^{\phi})_j \, (Y_n^{\phi t})_{ij} \\
(ZZ_n^{\phi t})_{ij} &= (Z_n^{\phi t})_{ij} - (Z_s^{t})_j \, (Y_n^{t\phi})_{ij} \\
(ZZ_n^{\phi\phi})_{ij} &= (Z_n^{\phi\phi})_{ij} + (Z_s^{\phi})_j \, (Y_n^{tt})_{ij}
\end{aligned}
\tag{3.29}
$$

The matrix elements for $[YY_n]$ are the same as those for $[ZZ_n]$ but with the roles of $[Z_n]$ and $[Y_n]$ on the right hand side of 3.19 interchanged.

As in the perfect conductor case, once each matrix equation is solved for the $[I_n]$, then that Fourier mode contribution to the scattered field can be calculated. In the IBC case, however, both $\hat{J}$ and $\hat{M}$ contribute to the scattered field. The next section will consider how to generalize the far field calculation algorithms of Mautz and Harrington to include the contribution of $\hat{M}$.

3.4 Generalization of Far Field Calculations

In general, the scattered electric field due to equivalent electric and magnetic sources $(\hat{J},\hat{M})$ on a surface can be expressed as:[15]

$$\hat{E}^s = -j\omega\mu \hat{A} - \nabla V - \nabla \times \hat{F} \tag{3.30}$$

where

$$\vec{A} = \int_s \vec{J}(\vec{r}')\, \Phi\, ds' \quad \text{(electric vector potential)}$$

$$V = -\int_s \frac{1}{j\omega} [\nabla' \cdot \vec{J}(\vec{r}')]\, \Phi\, ds' \quad \text{(scalar potential)}$$

$$\vec{F} = \int_s \vec{M}(\vec{r}')\, \Phi\, ds' \quad \text{(magnetic vector potential)}$$

At a far field point, defined by the spherical coordinates (r,θ,ϕ) and unit vectors $(\hat{r},\hat{\theta},\hat{\phi})$, Eq. 3.30 can be approximated as:[15]

$$\vec{E}^s(\vec{r}) = E_\theta^s\, \hat{\theta} + E_\phi^s\, \hat{\phi}$$

where:

$$E_\theta^s = -jk\eta \frac{e^{-jkr}}{4\pi r} \int_s [\vec{J}(\vec{r}')\cdot\hat{\theta} + \frac{1}{\eta} \vec{M}(\vec{r}')\cdot\hat{\phi}]\, e^{-jk\hat{r}\cdot\hat{r}'} ds'$$

$$E_\phi^s = -jk\eta \frac{e^{-jkr}}{4\pi r} \int_s [\vec{J}(\vec{r}')\cdot\hat{\phi} - \frac{1}{\eta} \vec{M}(\vec{r}')\cdot\hat{\theta}]\, e^{-jk\hat{r}\cdot\hat{r}'} ds' \qquad (3.31)$$

Mautz and Harrington define measurement matrices, $[R_n]$, having the elements:

$$R_{ni}^{pq} = k \int dt'\, \rho' f_i(t') \int_o^{2\pi} d\phi' (\hat{p}\cdot\hat{q})\, e^{j[-k\,\hat{r}\cdot\hat{r}' + n(\phi'-\phi)} \qquad (3.32)$$

where ρ' is the cylindrical coordinate ρ on the surface (a function of t') and where:

$p = t$ or ϕ	surface coordinate
$q = \theta$ or ϕ	spherical coordinate

Using 3.32 and the expansions for $\hat{J}$ and $\hat{M}$, the far scattered field components can be written as:

$$E_\theta^s = -j\eta \frac{e^{-jkr}}{4\pi r} \sum_n \sum_i [R_{ni}^{t\theta} I_{ni}^t + R_{ni}^{\phi\theta} I_{ni}^\phi + \frac{1}{\eta} R_{ni}^{t\phi} M_{ni}^t + \frac{1}{\eta} R_{ni}^{\phi\phi} M_{ni}^\phi] e^{jn\phi} \quad (3.33)$$

$$E_\phi^s = -j\eta \frac{e^{-jkr}}{4\pi r} \sum_n \sum_i [R_{ni}^{t\phi} I_{ni}^t + R_{ni}^{\phi\phi} I_{ni}^\phi - \frac{1}{\eta} R_{ni}^{t\theta} M_{ni}^t - \frac{1}{\eta} R_{ni}^{\phi\theta} M_{ni}^\phi] e^{jn\phi} \quad (3.34)$$

Using equation 3.16 for the elements of $[M_n]$, one obtains:

$$E_\theta^s = -j\eta \frac{e^{-jkr}}{4\pi r} \sum_n \sum_i [S_{ni}^{t\theta} I_{ni}^t + S_{ni}^{\phi\theta} I_{ni}^\phi] e^{jn\phi} \quad (3.35)$$

$$E_\phi^s = -j\eta \frac{e^{-jkr}}{4\pi r} \sum_n \sum_i [S_{ni}^{t\phi} I_{ni}^t + S_{ni}^{\phi\phi} I_{ni}^\phi] e^{jn\phi}$$

where

$$
\begin{aligned}
S_{ni}^{t\theta} &= R_{ni}^{t\theta} + (Z_s^t)_i \, R_{ni}^{\phi\phi} \\
S_{ni}^{\phi\theta} &= R_{ni}^{\phi\theta} - (Z_s^{\phi})_i \, R_{ni}^{t\phi} \\
S_{ni}^{t\phi} &= R_{ni}^{t\phi} - (Z_s^t)_i \, R_{ni}^{\phi\theta} \\
S_{ni}^{\phi\phi} &= R_{ni}^{\phi\phi} + (Z_s^{\phi})_i \, R_{ni}^{t\theta}
\end{aligned}
\tag{3.36}
$$

Since the moment-method programs of Mautz and Harrington calculate the elements of $[R_n]$, the $[S_n]$ elements can easily be calculated and the remainder of the far field calculation is essentially the same as described in Ref. 12.

4.0 NUMERICAL RESULTS

4.1 Introduction and Definitions

Presented in this section are numerical solutions to the IBC integral equations for scattering from impedance spheres. The primary objective is to contrast the EFIE, MFIE and CFIE formulations in terms of solution accuracy and stability. A second objective is to determine the sensitivity of the CFIE to parameters such as integral equation weighting coefficient (α) and moment-method segmentation (SEG) for different types of impedance surfaces (i.e. perfectly conducting, lossy, reactive, etc.).

The sphere surfaces are assumed to be characterized by a scalar, constant value of normalized surface impedance (Z_s). Specific values of Z_s are chosen to represent various types of impedance surfaces that might be encountered in scattering problems.[1-7,9] For example, a pure real value of Z_s could represent the surface impedance of a Salisbury screen type of configuration.[17] The special case of Z_s=1.0 (ideal Salisbury screen) is of interest since the flat plate reflection coefficient at normal incidence is zero. A pure imaginary value of Z_s could represent the surface impedance of a rough perfectly conducting surface or a perfect conductor coated with lossless dielectric layers. Reactive values of Z_s can allow surface wave resonances to exist where the scattering cross

section might change by 20 to 30 dB for a very small change in frequency. Bodies with finite conductivity or perfect conductors coated with lossy layers can be represented by values of Z_s having both real and imaginary parts. For example Z_s=0.1+j0.1 could represent the surface impedance of a homogeneous, lossy conductor or a perfect conductor coated with a thin lossy dielectric layer. Z_s=1.0+j1.0 might represent a conductor coated with a thick lossy layer.

The numerical results are presented in three parts. Section 4.2 contains examples of scattering from a perfectly conducting sphere (Z_s=0.0) for ka values in the vicinity of the first theoretical sphere interior resonance (ka=2.744). These results, which are similar to those of previous researchers[7,11,12], review present understanding of the effects of spurious resonances upon the stability and accuracy of moment-method solutions to the perfect conductor EFIE, MFIE and CFIE formulations. Also, the results demonstrate general properties of the convergence of moment-method solutions as a function of body segmentation and review techniques for determining the best choice of α in the CFIE. In Section 4.3, examples pertaining to scattering from impedance spheres are presented which demonstrate the influence of non-zero values of Z_s upon the convergence of solutions to the CFIE. Also, the problem of determining the best choice of α for non-zero values

of Z_s is considered in this section. Finally, Section 4.4 contains numerical examples which directly compare the stability and accuracy of scattering solutions of the EFIE, MFIE and the CFIE for non-zero values of Z_s at ka values near theoretical interior sphere resonances. The examples include backscatter vs ka near the first sphere resonance for Z_s=0.1+j0.1 and Z_s=1.0, backscatter vs. Re(Z_s) or Im(Z_s) at ka=2.75 and bistatic scattering from a sphere having Z_s=1.0 at ka values near each of the first four sphere resonances.

For purposes of definition, the term "stability" of a moment-method solution refers to the potential for numerical errors in the matrix equation which approximates the integral equation. A quantitative measure of solution stability which is used in all examples is the matrix condition number (described in the next few paragraphs). The term "accuracy" refers to the final solution (cross-section) accuracy. The moment-method solution accuracy for these sphere examples is determined by comparison with the Mie series solution (computed for each example using an independent computer program based on Ref. 14).

As stated above, a matrix condition number is used as a measure of the stability of the moment-method solutions. Consider the matrix equation Ax=y where A is a square matrix and x and y are column matrices (or vectors). When x is unknown and y is known, the solution is obtained by calculating $A^{-1}y$. An

error in the calculation of y of δy will produce an error in x of δx. When δy is in the direction of an eigenvector of A, it follows from Ax=y that δx will be in the direction of the same eigenvector. From the definition of matrix and vector norms, the relative uncertainty in x can be related to that of y by (assuming no uncertainty in the calculation of A or A^{-1}):[18]

$$\frac{||\ \delta x\ ||}{||\ x\ ||} \leq \text{cond}\ (A)\ \frac{||\ \delta y\ ||}{||\ y\ ||} \tag{4.1}$$

where cond(A), or condition number of A, is defined as:

$$\text{cond}(A) = ||A|| \cdot ||A^{-1}|| \tag{4.2}$$

and where $||\ \ ||$ denotes matrix norm when applied to A and vector norm when applied to x or y. When A is real and symmetric and when the geometric vector norm is used (length of the vector), cond(A) is the ratio of the maximum to the minimum eigenvalues of A.[18] If A is near singular (i.e. minimum eigenvalue near zero) cond(A) becomes very large. In such a case, an error δx in the direction of the eigenvector associated with the minimum eigenvalue may be large and perhaps may dominate the numerical solution for x.[18] Thus, cond(A) can be interpreted as an amplification factor for numerical errors in solving a matrix equation. For example, a condition number of 1000 means that the expected relative uncertainty in the solution x is 1000 times that of y.

To connect the above discussion with the impedance body scattering formulations, recall that the calculation of cross section described in Section 3 is a two-step process. First the integral equation (EFIE, MFIE or CFIE) is approximated by a matrix equation to obtain a discrete representation of the equivalent currents on the body surface. Then the scattered field due to these equivalent currents is computed by a closed surface integration. The condition numbers of the matrix approximation to the IBC integral equations characterize the stability of the first half of the calculation of cross-section. That is, the condition numbers reflect the probable errors in the equivalent currents - not necessarily the same as the relative errors in cross section. For the EFIE and MFIE formulations, when at a frequency near a spurious resonance, the integral operators are near singular and matrix approximations are ill-conditioned. By analogy with the example of the real, symmetric matrix, the probable errors in the equivalent currents are the equivalent currents of the interior resonance problem.

For the results in this report, cond(A) is determined using the infinity norm definition - which is much easier to calculate than the geometric norm but has a more difficult geometrical interpretation.[18] To accomplish this calculation, the matrix decomposition and solution routines of Ref. 13 are replaced by those of Ref. 19. Also, for all examples axial incidence to the spheres are assumed (without loss of generality). In this case

only the M=1 Fourier mode of the moment-method solution is non-zero and solution stability is characterized by a single condition number.

For purposes of quantifying solution accuracy in some examples, a mean percentage error (ME) in the bistatic cross section is defined as follows:

$$ME = \frac{1}{N} \sum_{n=1}^{N} \left| \frac{\sigma_{cfie}(\theta_n) - \sigma_{mie}(\theta_n)}{\sigma_{mie}(\theta_n)} \right| \times 100\%$$

In the above equation, θ_n is a bistatic angle and N is the total number of bistatic angles used. For all examples, N=362 (181 E-plane and 181 H-plane angles). σ_{cfie} represents the bistatic cross section of the CFIE equation and σ_{mie} is the Mie series solution. Since the above definition blows up when σ_{mie} becomes very small, for any value of $\sigma/\pi a^2 \leq 10^{-5}$, a value of 10^{-5} is used. This modification is only required for the examples of Z_s=1.0 at small bistatic angles.

As an aid to interpreting the ME, Fig. 4.1 shows four examples E-plane bistatic scattering patterns for an impedance sphere with Z_s=1.0+j1.0 and ka=2.75. Different values of α result in different degrees of solution accuracy. These bistatic scattering patterns show that for a given ME, larger percentage errors occur near backscattering while smaller percentage errors occur near forward scattering.

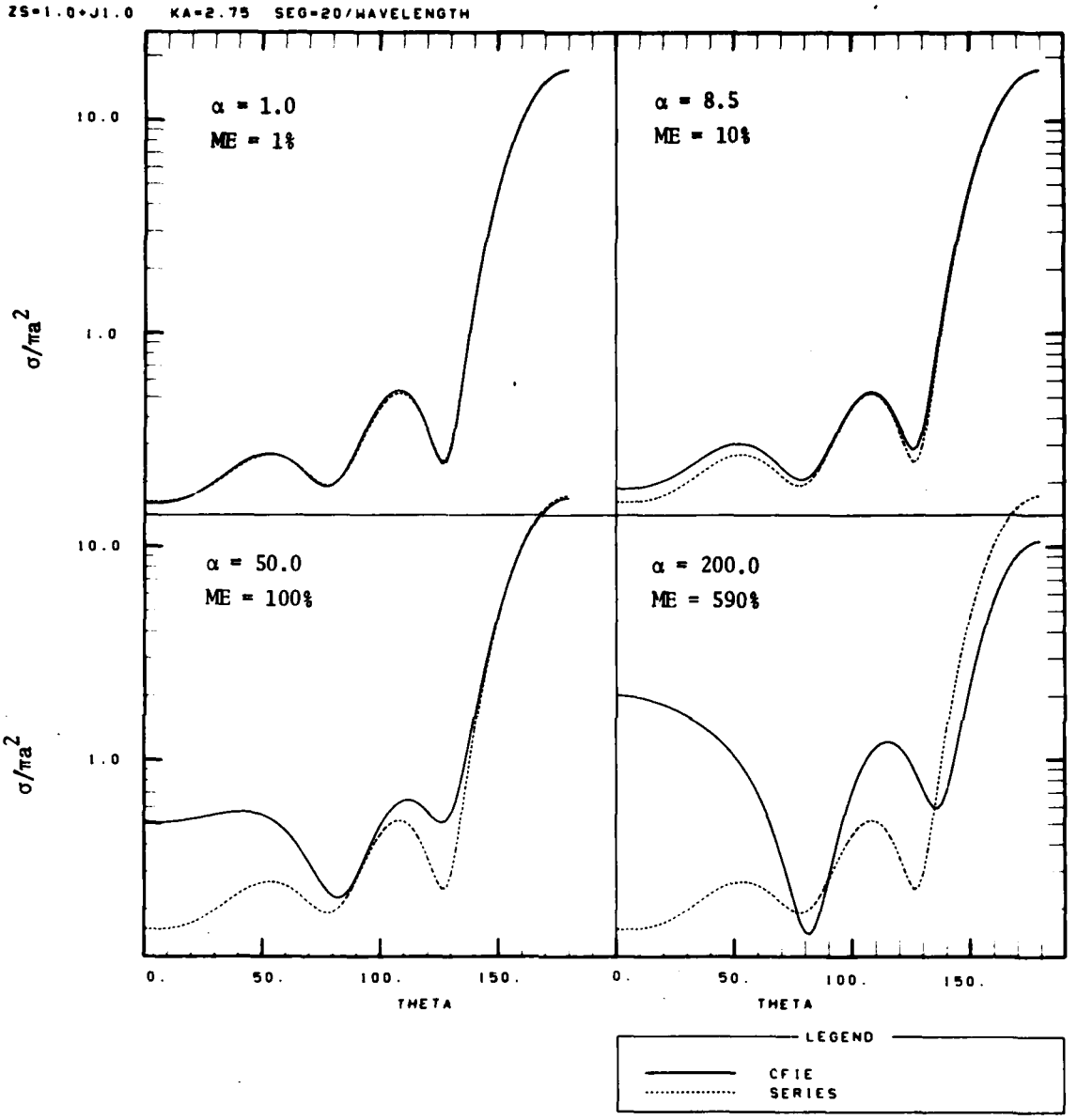

Fig. 4.1. Example E-plane bistatic scattering patterns illustrating different degrees of solution accuracy and the corresponding values of mean error (ME).

4.2 Perfectly Conducting Sphere Examples

This section contains numerical examples applicable to scattering from perfectly conducting spheres (Z_s=0.0). The purposes of first presenting these examples are to: (1) provide a reference for comparing the scattering examples in which Z_s is non-zero, (2) illustrate general criteria concerning convergence of a moment-method solution, (3) review current understanding of the effects of spurious resonant solutions on the EFIE and MFIE, and (4) review methods for determining a suitable choice of integral equation weighting coefficient (α) in the CFIE. Some of these examples have been considered in detail by Oshiro, et. al.[7] and Mautz, et. al.[11-13]

Figure 4.2 illustrates the effect of increasing moment-method segmentation (SEG) upon the accuracy and stability of solutions to the EFIE, MFIE and CFIE (α=.25) at ka=2.50. Plotted are the bistatic cross section mean error (ME) and condition number (cond) vs. SEG. An alternate abscissa is provided below the figure to indicate matrix sizes. SEG is defined as the number of straight-line body profile segments per wavelength. The number of expansion functions per wavelength is approximately SEG/2. In the figure, the ordinates that increase with increasing SEG are condition numbers and the ordinates that decrease are mean errors. α=.25 is used for the CFIE solutions following guidelines established in the literature[7,11-13]

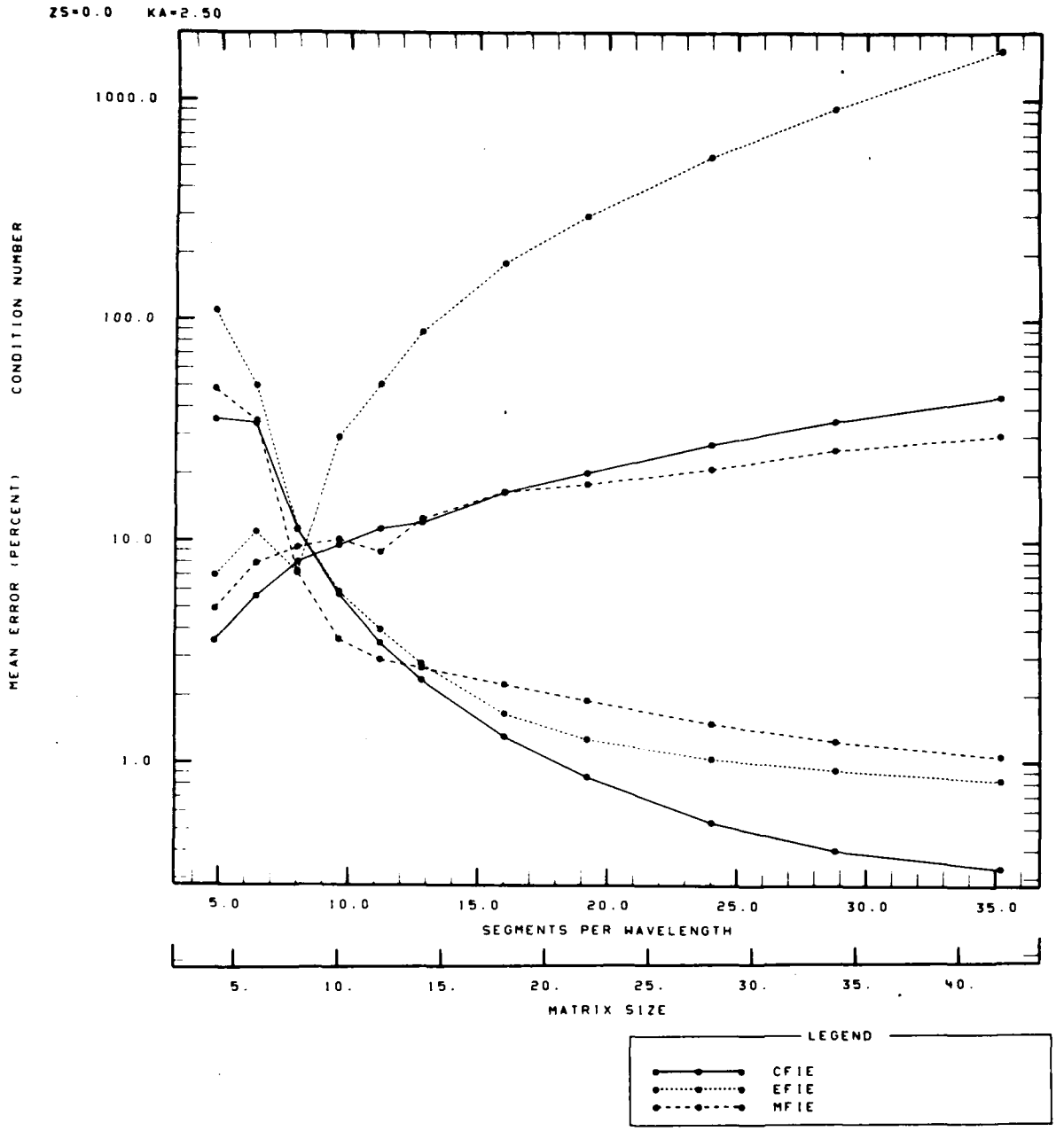

Fig. 4.2. Mean error in the perfectly conducting sphere bistatic cross section (decreasing ordinates) and condition number (increasing ordinates) vs. moment-method segmentation or matrix size (ka = 2.50).

(an example showing how a suitable choice of α can be determined is presented later in this section).

At this value of ka the EFIE, MFIE and CFIE behave similarly as SEG is increased - that is the accuracy of each equation improves and the condition numbers of each equation increase. The improvement in accuracy is due to the finer moment-method segmentation allowing a better approximation to the equivalent currents while the increase in condition numbers is due to the larger matrix sizes having smaller minimum eigenvalues. If the segmentation is increased further and further, eventually a crossover point in improvement in accuracy would be reached beyond which the accuracy would worsen with increasing SEG.[20]

The accuracy of the three equations as described by the ME is comparable at any given SEG. However, the relative stabilities of the three equations at a given SEG are different. For matrix sizes larger than about 10 x 10, the EFIE is relatively ill- conditioned as compared to the MFIE and the CFIE (α=.25). This difference in conditionality is a result of the EFIE being a Fredholm integral equation of the 1st kind while the MFIE and CFIE (which is heavily weighted with the MFIE in this example) are second kind equations.[21] Briefly, as the matrix size increases due to finer moment-method segmentation, matrix elements obtained from integrals will decrease in magnitude since the surface area of integration decreases. In a 1st kind

equation (EFIE) all elements are calculated from terms involving surface integrals, and hence their magnitudes (and the magnitude of the minimum eigenvalue) decrease as the matrix size increases. As the matrix size tends toward infinity, the matrix elements of a 1st kind equation tend toward zero. In a 2nd kind equation (MFIE) a term exists which does not involve integration. Thus, the MFIE tends to become more diagonally dominant as the matrix size increases - with the diagonal elements in general tending toward non-zero values as the matrix size increases toward infinity.[21]

The relative values of condition number imply that the errors in the computed equivalent currents are probably greatest in the EFIE and least in the MFIE. In fact for some matrix sizes, the equivalent current errors in the EFIE solutions are probably an order of magnitude larger than those of the MFIE or the CFIE (α=.25). Yet the solution accuracy of the EFIE as described by the ME is generally better than the MFIE at a given SEG for ka=2.50. This apparant contradiction has been explained by examining the fields generated by spurious equivalent currents.[11,12] Resonant cavity equivalent currents of the form $(\vec{J},0)$ satisfy the boundary condition $\hat{n}x\vec{E}_-=0$ on S for the EFIE. Applying Eq. 2.1 (with $\vec{M}=0$), the resonant cavity equivalent currents satisfy $\hat{n}x\vec{E}_+=0$ which implies $\hat{n}x\vec{H}_+=0$ when radiation conditions are met. Thus the spurious equivalent currents which

enter scattering solutions to the perfect conductor EFIE have zero exterior electromagnetic fields. If calculated exactly, these spurious currents do not contribute to the computation of scattered field. In contrast, resonant cavity equivalent currents of the MFIE of the form $(\vec{J},0)$ satisfy $\hat{n}x\vec{H}_-=0$ - which implies $\hat{n}x\vec{H}_+=\vec{J}$ and $\hat{n}x\vec{E}_+\neq 0$. These resonant currents are non-physical but never-the-less exist when enforcing $\hat{n}x\vec{H}_-=0$. Thus, spurious equivalent currents of the MFIE have non-zero exterior fields and hence contribute directly to the computed scattered field. The net result is that the final solution accuracies of the EFIE and the MFIE are comparable even though the computed equivalent currents of the EFIE contain much larger errors than those of the MFIE (verified by Mautz through actual computation of currents in the sphere examples).

Figures 4.3 a and b illustrate the relative accuracies and stabilities respectively of solutions to the EFIE, MFIE and CFIE (α=.25) for a range of ka values near the first theoretical sphere resonance (ka=2.744). Plotted in Fig. 4.3a is normalized backscatter ($\sigma/\pi a^2$) from a perfectly conducting sphere vs. ka as predicted by each of the integral equations and the Mie series. The matrix size is 26 x 26 for all points which corresponds to a SEG of approximately $20/\lambda$. Figure 4.3a demonstrates the regions of inaccuracy in the EFIE and MFIE and the potential errors in magnitude in computing backscatter at

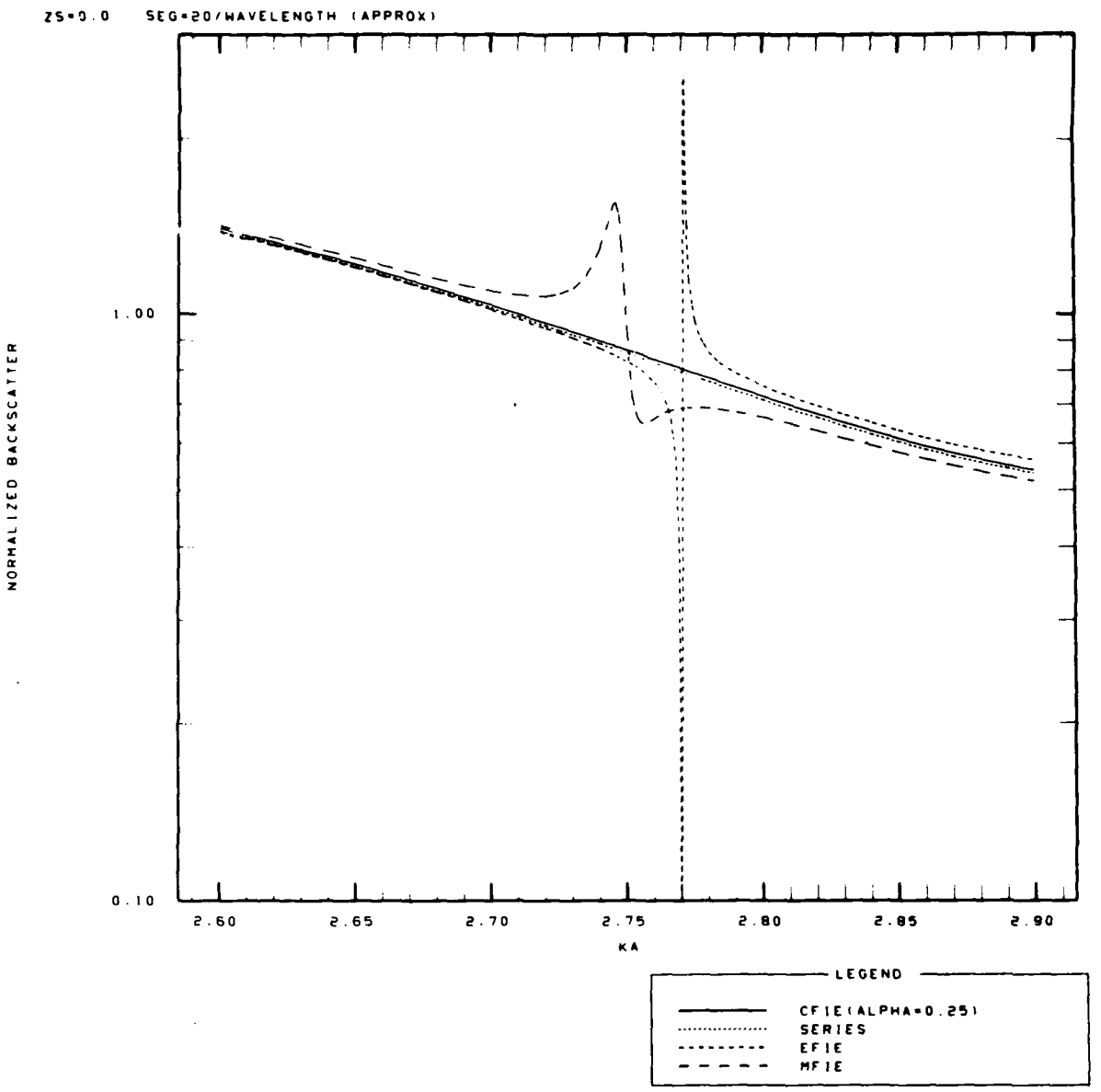

Fig. 4.3a. Normalized backscatter ($\sigma/\pi a^2$) from a perfectly conducting sphere vs. normalized wavenumber (ka) for ka values near the first theoretical sphere interior resonance (ka = 2.744). Segmentation (SEG) is defined as the number of straight-line body profile segments per wavelength.

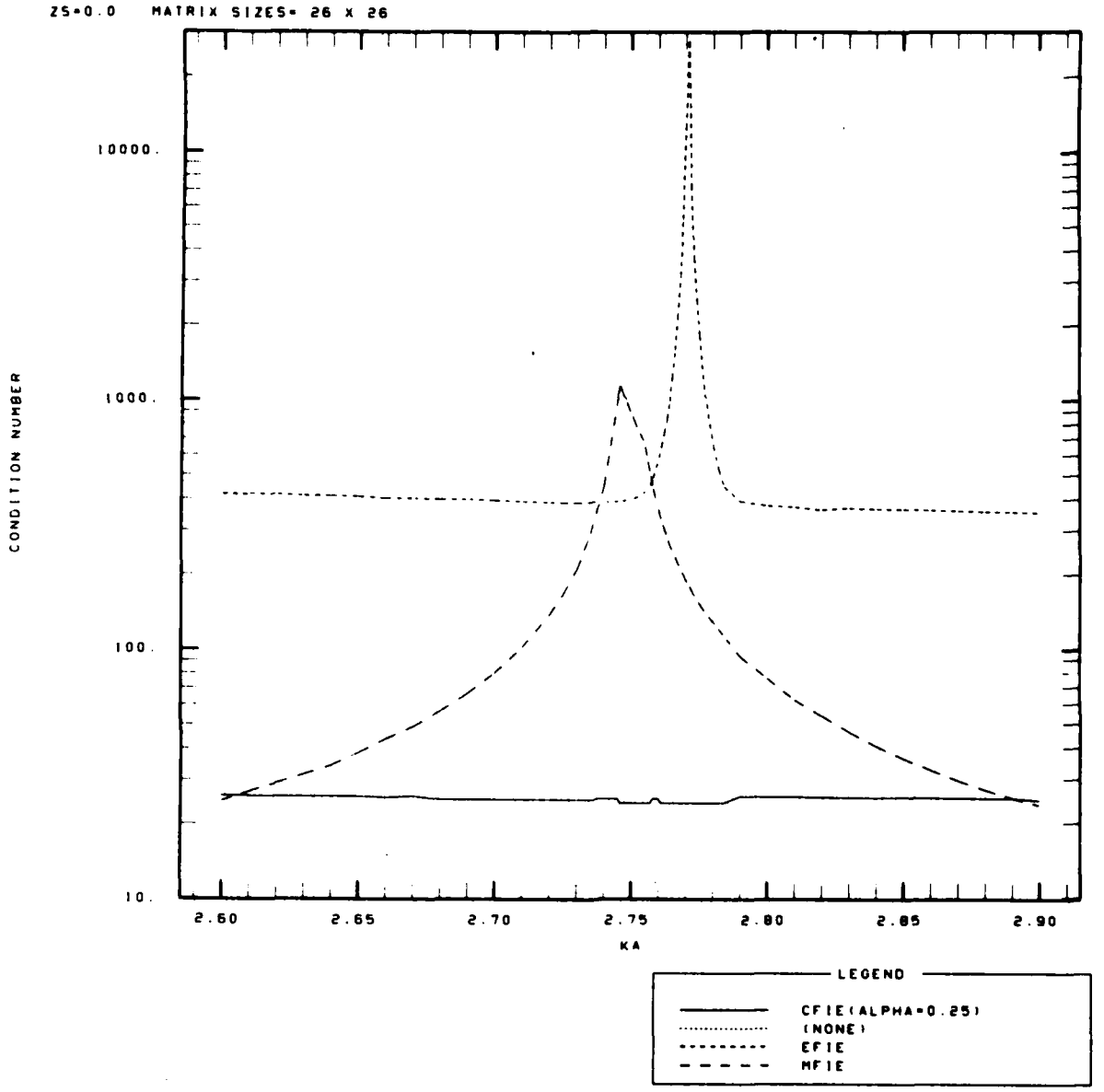

Fig. 4.3b. Matrix condition numbers (m = 1 Fourier mode) for the perfectly conducting sphere of Fig. 4.3a vs. ka.

SEG=20λ. Plotted in Fig. 4.3b are the condition numbers which correspond to the data of Fig. 4.3a. These values of cond indicate the regions of instability and the relative errors in the equivalent currents of solutions to the three integral equations.

Figures 4.3a and b both indicate that the EFIE and MFIE are affected by (or predict the location of) the spurious resonance at different ka values. By virtue of its inherent better conditioning, the MFIE predicts the resonance closer to the theoretical value. Figures 4.3a and b also indicate that the 1st sphere interior resonance affects the MFIE over a broader range of ka values than the EFIE (i.e., the MFIE has a wider bandwidth for errors). However, the largest potential magnitude of errors in backscatter from the sphere appears to occur for the EFIE in a very narrow range of ka values. Throughout the region of the interior sphere resonance, the CFIE (α=.25) gives accurate scattering predictions and demonstrates no ill-conditioning from the resonance.

Figure 4.4 shows the effect of changing matrix size on the scattering predictions of the EFIE near the first sphere resonance. In this figure, normalized backscatter from a perfectly conducting sphere vs. ka is plotted using three different matrix sizes in the EFIE solution - 6 x 6 (SEG≈7/λ), 12 x 12 (SEG≈10/λ) and 26 x 26 (SEG≈20/λ). The dashed ordinate is the Mie series solution. As matrix size increases, three

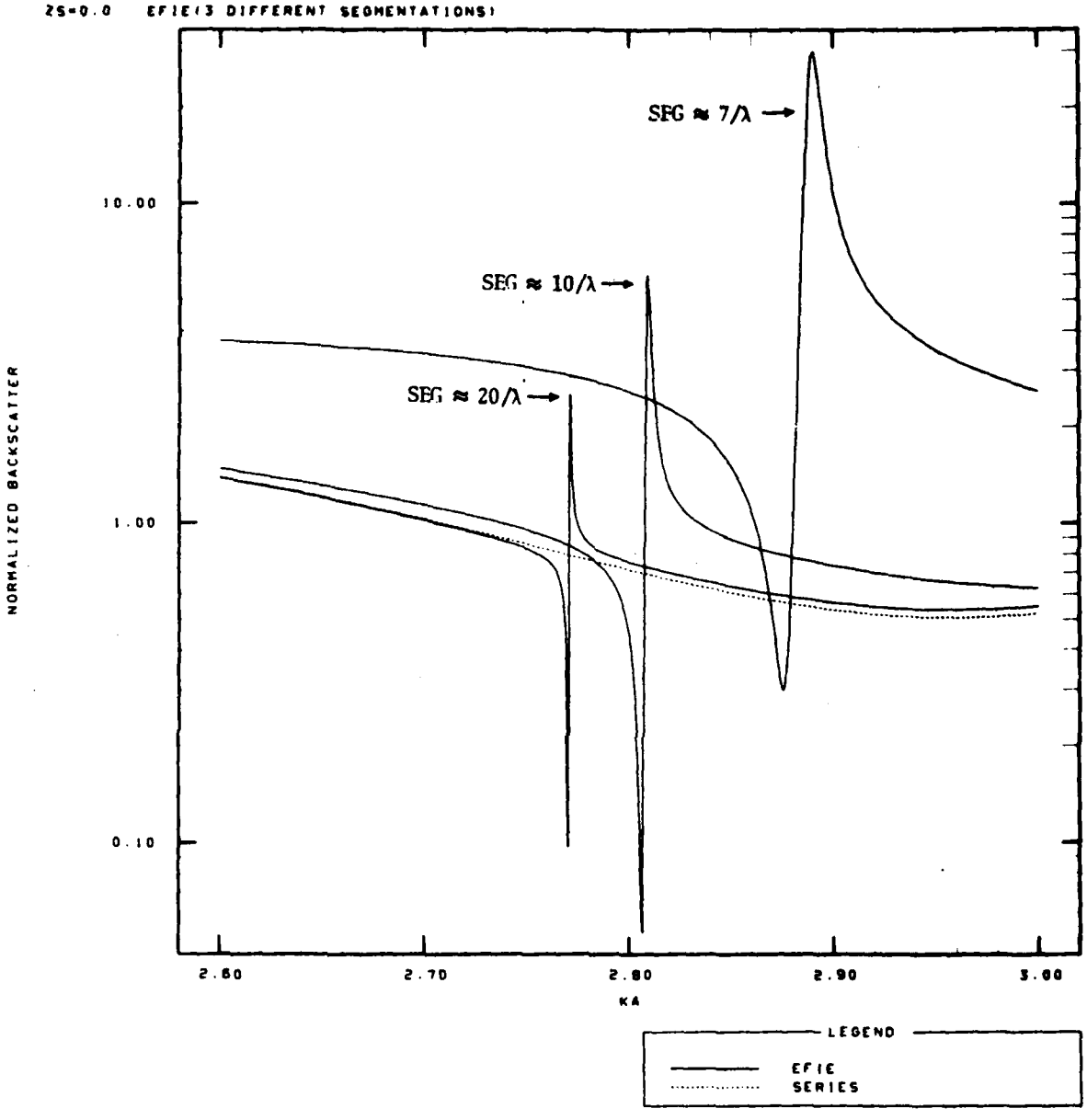

Fig. 4.4. Effect of changing moment-method segmentation on the normalized backscatter vs. ka predictions of the EFIE (perfectly conducting sphere).

effects can be seen upon the contamination of the EFIE scattering solutions by the spurious resonance. First, the magnitude of the potential errors decreases as matrix size increases. Secondly, the region of inaccuracy (bandwidth of errors) narrows as indicated by the shape of the curves. Thirdly, the predicted location of the resonance gets closer to the theoretical ka value as the matrix size increases. The MFIE scattering predictions (not shown in the figure) are affected in a similar manner - with the bandwidths for errors being wider than those of the EFIE at the same matrix size and the predicted location of the resonance being closer to the theoretical value at a given matrix size.

The problem of choosing a suitable value for the CFIE weighting coefficient (α) has been considered by Oshiro, et.al.[7] and Mautz, et.al.[11-13] for scattering from perfectly conducting spheres. Using a bistatic cross section mean error (very similar to the one used in this report), Oshiro determined the best choice of α to be in the range of .2 - .3 for a variety of ka values. Using the rms error in the equivalent current as the criterion (analogous to the condition numbers of this report), Mautz and Harrington determined the best choice of α to be approximately .2 for ka near the 1st sphere resonance.

Figure 4.5 illustrates the above two described methods by displaying ME and cond vs. α for 5 different ka values near the 1st sphere resonance. Matrix sizes are 26 x 26 which corresponds

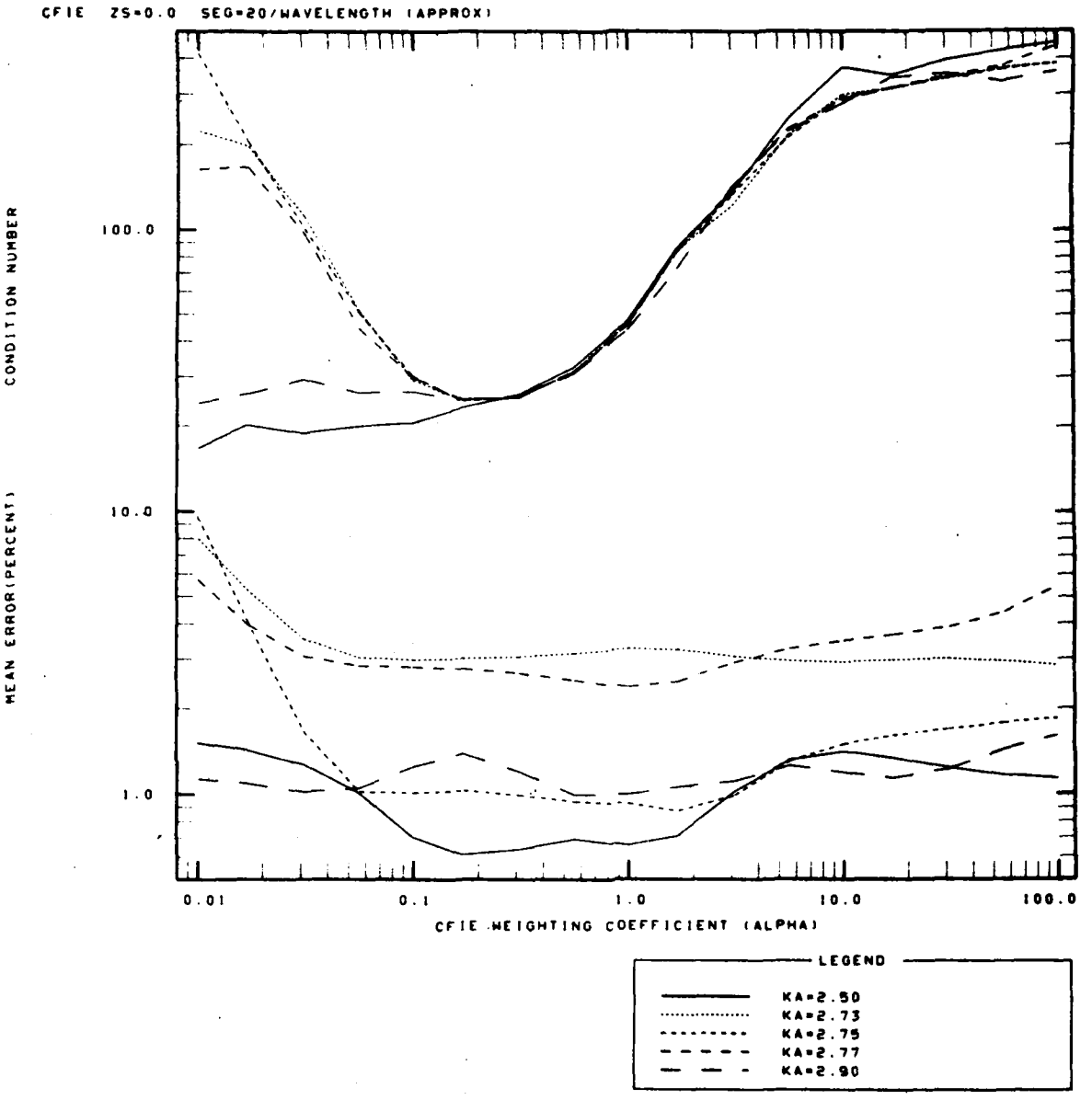

Fig. 4.5. Mean error in the perfectly conducting sphere bistatic cross section (lower set of ordinates) and the associated matrix condition numbers (upper set of ordinates) vs. CFIE weighting coefficient (α) for different ka values around ka = 2.744. Note: CFIE → MFIE as $\alpha \to 0$ and CFIE → EFIE as $\alpha \to$ infinity.

to SEG=20/λ. When α=.01, the CFIE solution can be considered near to the MFIE solution. When α=100.0, the CFIE solution is near an EFIE solution. The values of ME are all $\leq$ 10% - indicating that for SEG=20/λ good accuracy in the cross section can be obtained using almost any α (for perfectly conducting spheres). It appears that the range of .1 < α < 1.0 may be the best range to obtain good accuracy for any ka. The values of cond in Fig. 4.5 indicate that there exists a more narrow range of α values for obtaining the most well-conditioned matrices and smallest errors in the currents for all ka values of Fig. 4.5. Clearly, .2 < α < .3 is a range which gives well-conditioned matrices for all ka values near the 1st sphere resonance.

4.3 Influence Of Non-Zero Values Of Surface Impedance On Choice Of Integral Equation Weighting Coefficient And Moment-Method Segmentation For The Combined Field Integral Equation

The problems of choosing the CFIE weighting coefficient (α) and adequate moment-method segmentation (SEG) when calculating scattering from impedance spheres are considered in this section. The values of normalized surface impedance used for these numerical examples are Z_s=0.1+j0.1 (representing a thin lossy dielectric layer), Z_s=1.0+j1.0 (representing a thick lossy layer), Z_s=$\pm$j1.0 (representing lossless inductive and capacitive surfaces and Z_s=1.0 (representing an ideal Salisbury

screen). Choosing the best α is considered first for 2 ka values near the 1st sphere resonance assuming that SEG=20/λ is adequate segmentation. Using suitable choices of α for the different impedance surfaces, the convergence of the CFIE as a function of SEG is then examined at ka=2.75.

Figures 4.6a and b show respectively the accuracy and stability of the CFIE scattering solutions as a function of α at ka 2.50. ME vs. α is displayed in Fig. 4.6a and cond vs. α is displayed in 4.6b. Matrix sizes of the data in both figures are 26 x 26 (SEG=22/λ). For the values of Z_s considered, the solution accuracy as described by the ME is highly variable for a given matrix size. The best ME that could be achieved for $Z_s=\pm j1.0$ is about 7.2% - significantly worse than the perfectly conducting case of .062% (Fig. 4.2) at the same SEG. The values of ME in Fig. 4.6a also demonstrate that the functional dependence of solution accuracy on α is also highly variable depending on Z_s. For example, values of ME for $Z_s=\pm j1.0$ are relatively insensitive to α while values of ME when $Z_s=1.0$ are very sensitive to α. For this latter case, ME less than 10% is obtained only in a very narrow range of α around 1.0.

The condition numbers of Fig. 4.6b show that for a given matrix size and ka, the dependence of cond on α and the values of cond at a given α both appear to be dependent on Z_s. Only the case of $Z_s=0.1+j0.1$ was similar to the perfectly conducting case - where small α implied well-conditioned matrices (cond=20)

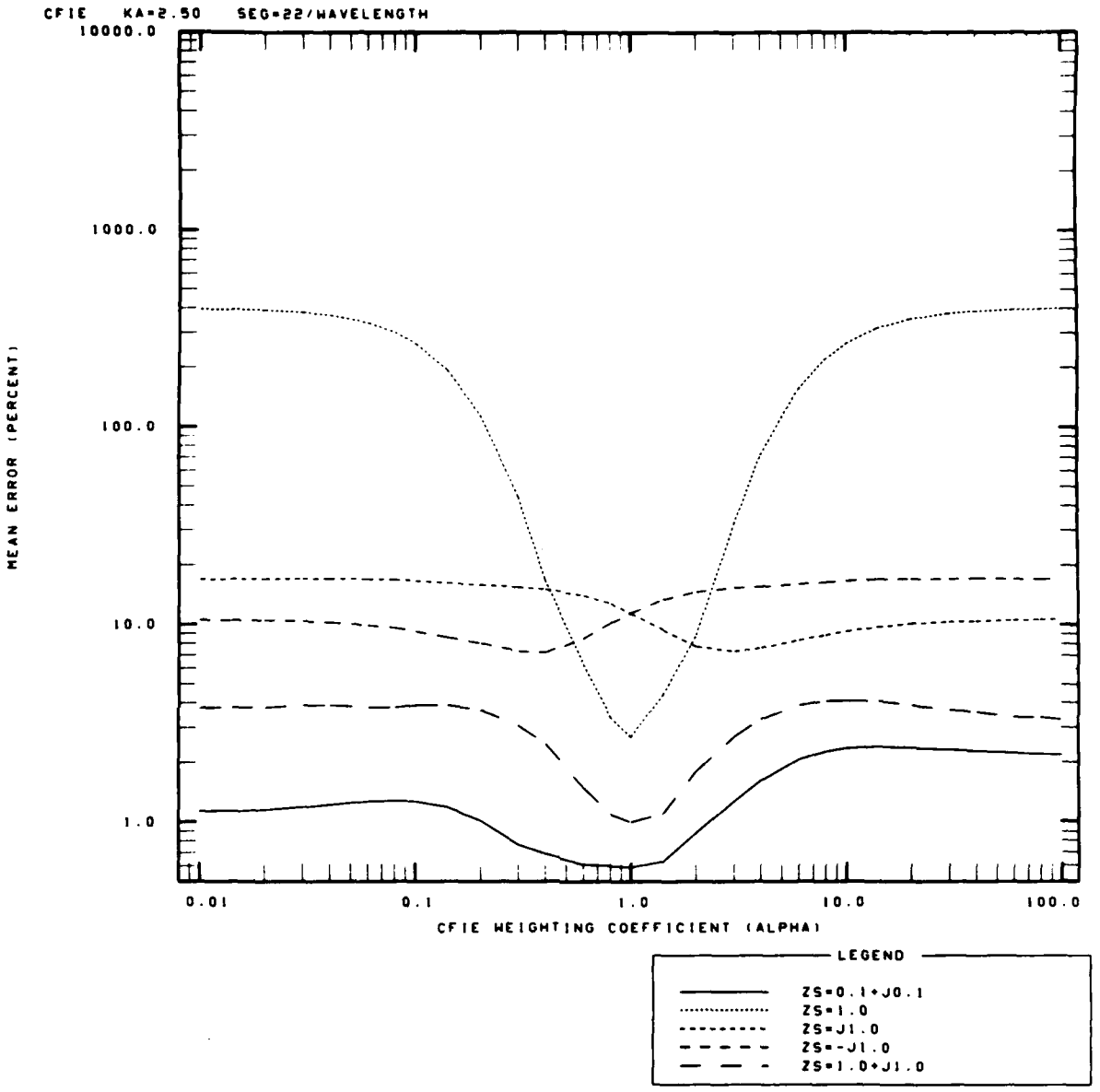

Fig. 4.6a. Mean error in the impedance sphere bistatic cross section vs. CFIE weighting coefficient (α) at ka = 2.50 assuming different values of normalized surface impedance (Z_s).

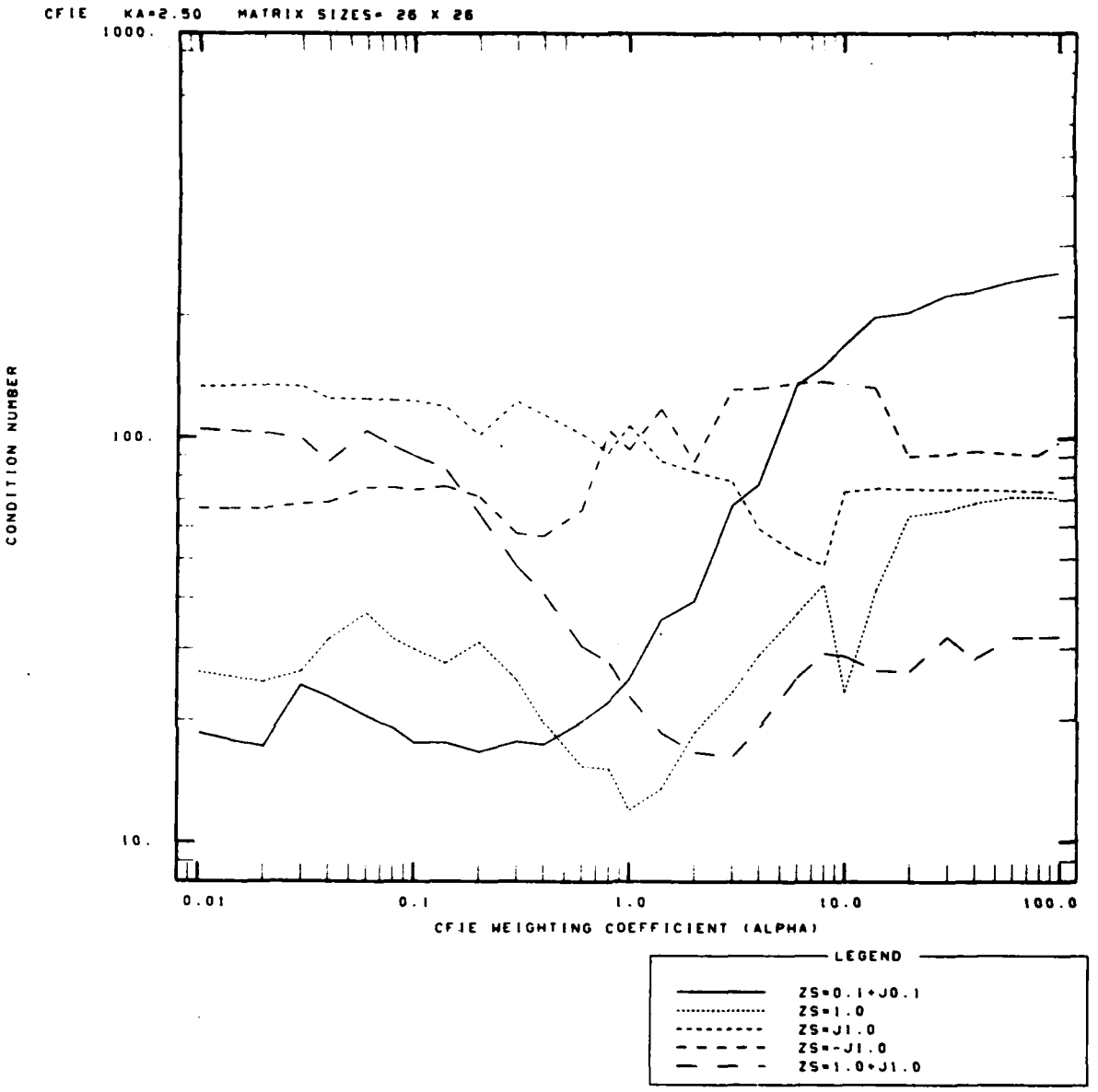

Fig. 4.6b. Matrix condition numbers (m = 1 Fourier mode) for the impedance sphere solutions of Fig. 4.6a vs. CFIE weighting coefficient (α).

and large α implied ill-conditioned matrices (cond 300 - 400). The influence of Z_s on the dependence of cond with α can be partly explained by observing that Z_s plays a similar role to that of when Z_s=0 (i.e., $\hat{M}$=0). That is, the ill-conditioned L_E operator (perfect conductor EFIE) is combined with the well-conditioned L_H operator (perfect conductor MFIE) in both the the EFIE and MFIE (see Eqs. 3.5 and 3.6). These two equations are then combined in the CFIE. However, when Z_s has an absolute value on the order of 1.0, the mix of the two perfect conductor operators is about the same in the CFIE regardless of α. Thus, the value of Z_s (or the type of impedance surface) also plays a role in the variability of the condition number at a given α.

Figures 4.7a and b display ME vs. α and cond vs. α respectively for ka=2.75. Matrix sizes are 26 x 26 - corresponding to SEG=20/λ. At this ka, very close to the 1st sphere resonance, the sensitivity to α of the CFIE solution accuracy and stability is noticeably increased over that at ka=2.50 (Figs. 4.6 a and b). Also, the best solution accuracy that is achieved for the pure reactive surface impedance cases (Z_s=$\pm$j1.0) is noticeably worse at ka=2.75 over that at ka=2.50. For these pure reactive cases, the best ME at SEG=20/λ is only about 10%. To obtain ME < 10%, choice of α is critical for Z_s=1.0 and Z_s=$\pm$j1.0. For Z_s=.1+j.1 and 1.0+j1.0,

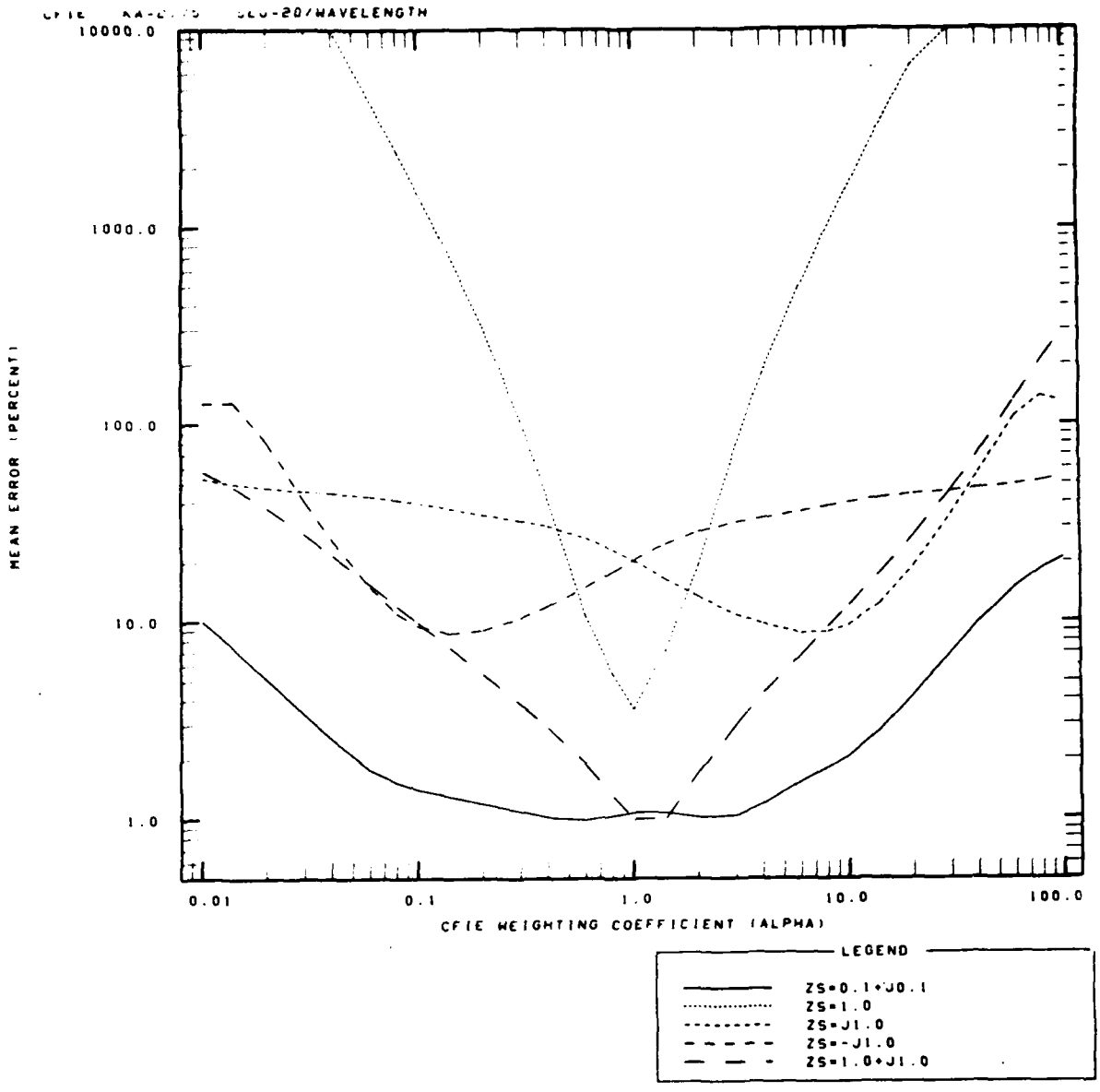

Fig. 4.7a. Mean error in the impedance sphere bistatic cross section vs. CFIE weighting coefficient (α) at ka = 2.75 for different values of normalized surface impedance.

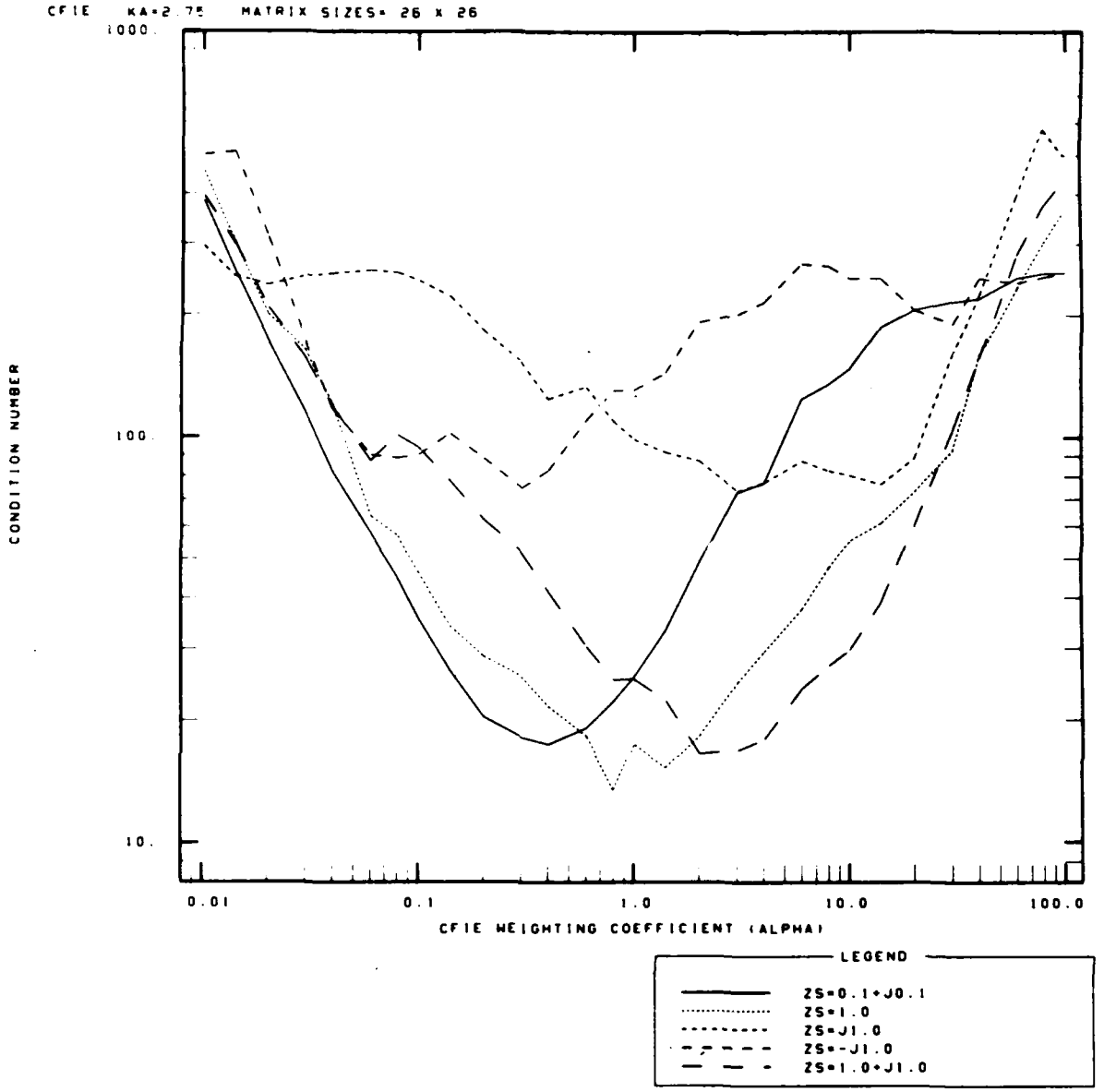

Fig. 4.7b. Matrix condition numbers (m = 1 Fourier mode) for the impedance sphere solutions of Fig. 4.7a vs. CFIE weighting coefficient (α).

the choice of α is less critical to obtain ME < 10%. However, even in these latter two cases, the choice of α is more important than in the perfectly conducting case (Fig. 4.5).

The final numerical example in this section considers the influence of non-zero surface impedance on the convergence of impedance sphere scattering solutions of the CFIE. Plotted in Figs. 4.8a and b respectively are ME vs. SEG and cond vs. SEG at ka=2.75 for the different values of Z_s. α is chosen to obtain close to the best solution accuracy at a given Z_s using Fig. 4.7a. The actual values of α used in Figs. 4.8a and b are:

Z_s	alpha
0.1+j0.1	0.6
1.0	1.0
j1.0	7.0
-j1.0	0.14
1.0+j1.0	1.25

The convergence of the CFIE as a function of moment-method segmentation is similar to the perfect conductor case (Fig. 4.2) in that increasing SEG generally improves solution accuracy. As SEG increases from $5/\lambda$ to $10/\lambda$ there is a rapid improvement in solution accuracy. For SEG > $20/\lambda$ improvement in accuracy is slow. Convergence of the CFIE for non-zero Z_s is different from the perfectly conducting case in that a given value of SEG does not guarantee that solution accuracy will be comparable to

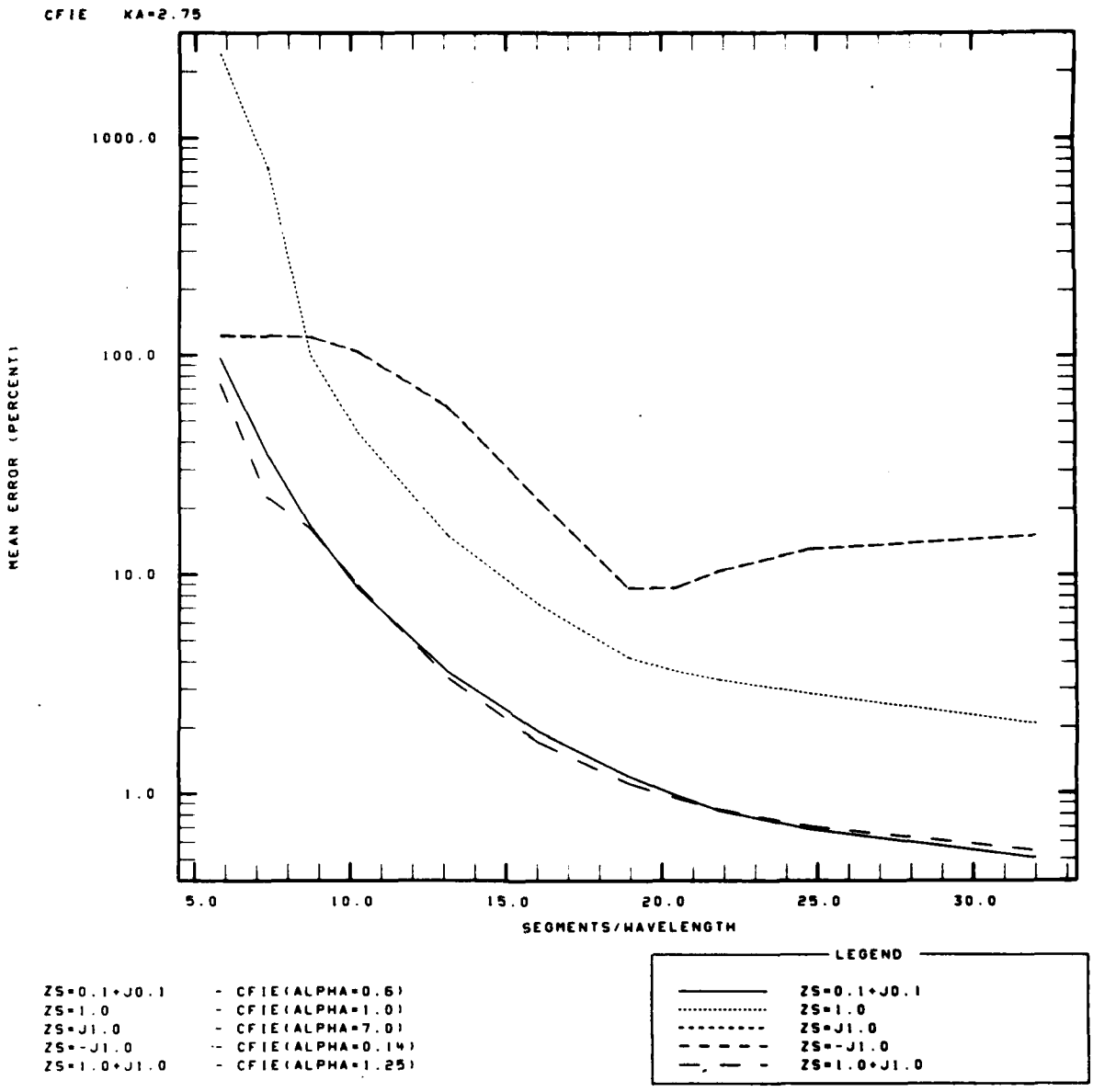

Fig. 4.8a. Mean error in the impedance sphere bistatic cross section vs. moment-method segmentation at ka = 2.75. Note: the $Z_s = \pm j1.0$ ordinates nearly overlay each other, apparently a consequence of $\alpha(Z_s = j1.0) = 1/\alpha(Z_s = -j1.0)$.

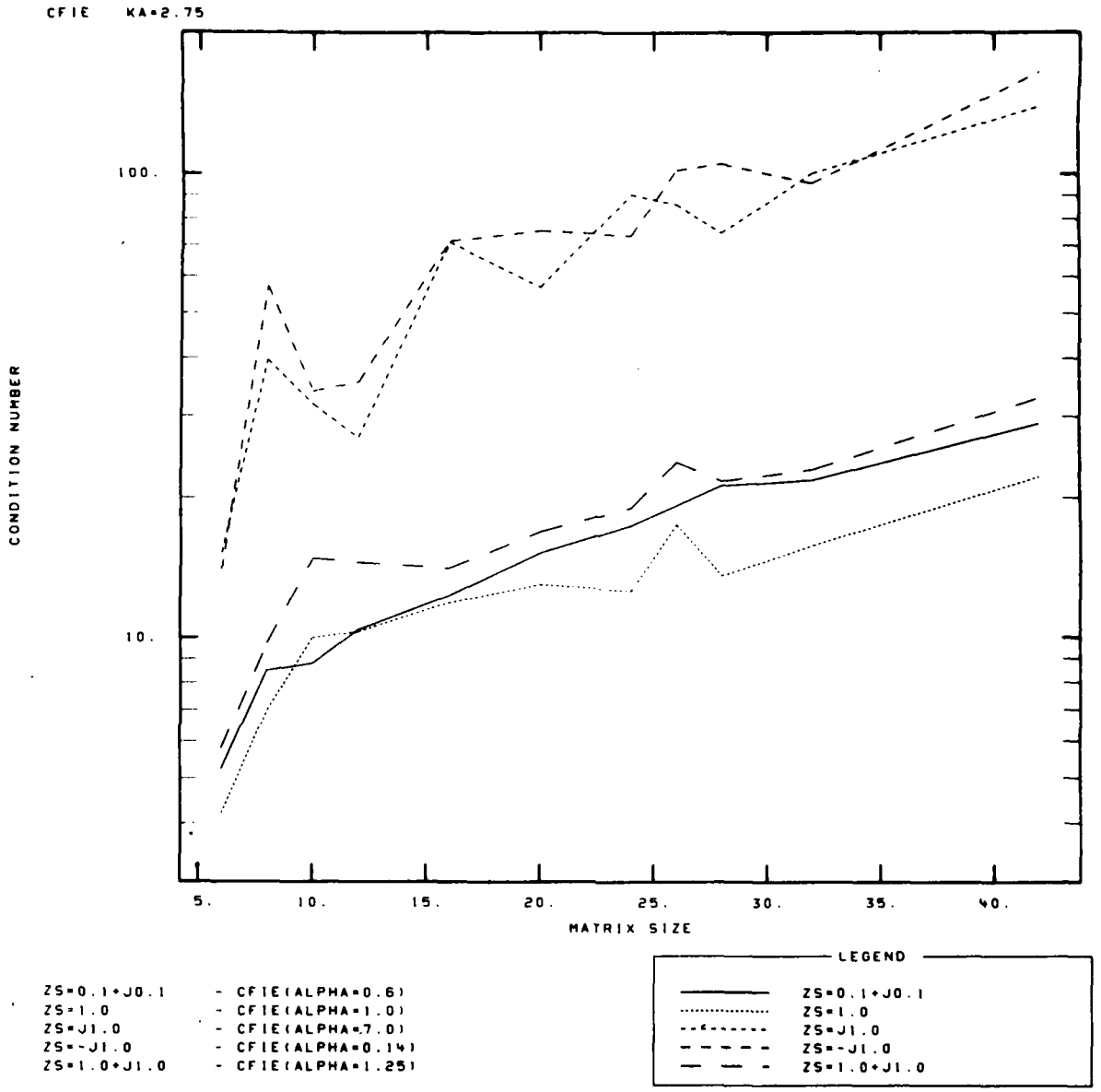

Fig. 4.8b. Matrix condition numbers (m = 1 Fourier mode) of the impedance sphere solutions of Fig. 4.8a vs. matrix size.

that of the perfectly case. This fact could also have been inferred from Figs. 4.6a and 4.7a for which all data points are at SEG=$20/\lambda$.

The convergence of the CFIE when $Z_s=\pm j1.0$ is interesting in two respects. First, the solutions are relatively inaccurate and the matrices are relatively ill-conditioned when $Z_s=\pm j1.0$ as compared to the other cases of Z_s. Secondly, for SEG > $20/\lambda$ there is actually an increase in mean errors with increasing SEG while for the other values of Z_s there is a gradual decrease in ME. The increase in ME with increasing SEG for the pure reactive cases suggests that the best choice of α changes when SEG is changed. However, this possibility was determined not to be the reason for the convergence behavior for $Z_s=\pm j1.0$ exhibited in Fig. 4.8a. The best choice of α was determined for $Z_s=j1.0$ at SEG=$32/\lambda$ (matrix sizes=45 x 45) by generating a curve similar to the one for SEG=$20/\lambda$ in Fig. 4.7a. The results were that the best choice of α remained at approximately 7.0 with the lowest ME approximately 15%. Thus, it appears that the cross-over point at which there is no longer improvement in accuracy with increasing matrix size occurs very early for $Z_s=\pm j1.0$ at ka=2.75.

4.4 Comparison Of the Electric, Magnetic and Combined Field Integral Equations For Non-Zero Values Of Surface Impedance

Examples of scattering from impedance spheres are presented in this section which directly compare solutions to the EFIE and MFIE with those of the CFIE for ka values near spurious resonances. The primary objective of this section is to demonstrate that spurious resonant solutions can severely contaminate the EFIE and MFIE predictions of exterior scattering from impedance bodies while the CFIE is a formulation which rejects the spurious solutions.

Backscattering from a sphere with with $Z_s=0.1+j0.1$ at ka values near the first sphere resonance is considered in Figs. 4.9a and b. Normalized backscatter vs. ka as predicted by the EFIE, MFIE, CFIE ($\alpha=.6$) and Mie series is plotted in Fig. 4.9a and condition numbers for the integral equations vs. ka in Fig. 4.9b. Matrix sizes of the data are 26 x 26 which corresponds to $SEG \approx 20/\lambda$. The scale sizes of Figs. 4.9a and b are the same as those of Figs. 4.3a and b to allow direct comparison with the perfectly conducting case.

The presence of the non-zero surface impedance causes some subtle changes in the accuracy and stability of the integral equation solutions relative to the perfectly conducting case. First, the bandwidth for errors and the magnitude of errors in the EFIE and MFIE cross sections are larger than in the perfectly conducting case. This is just the opposite that one would expect

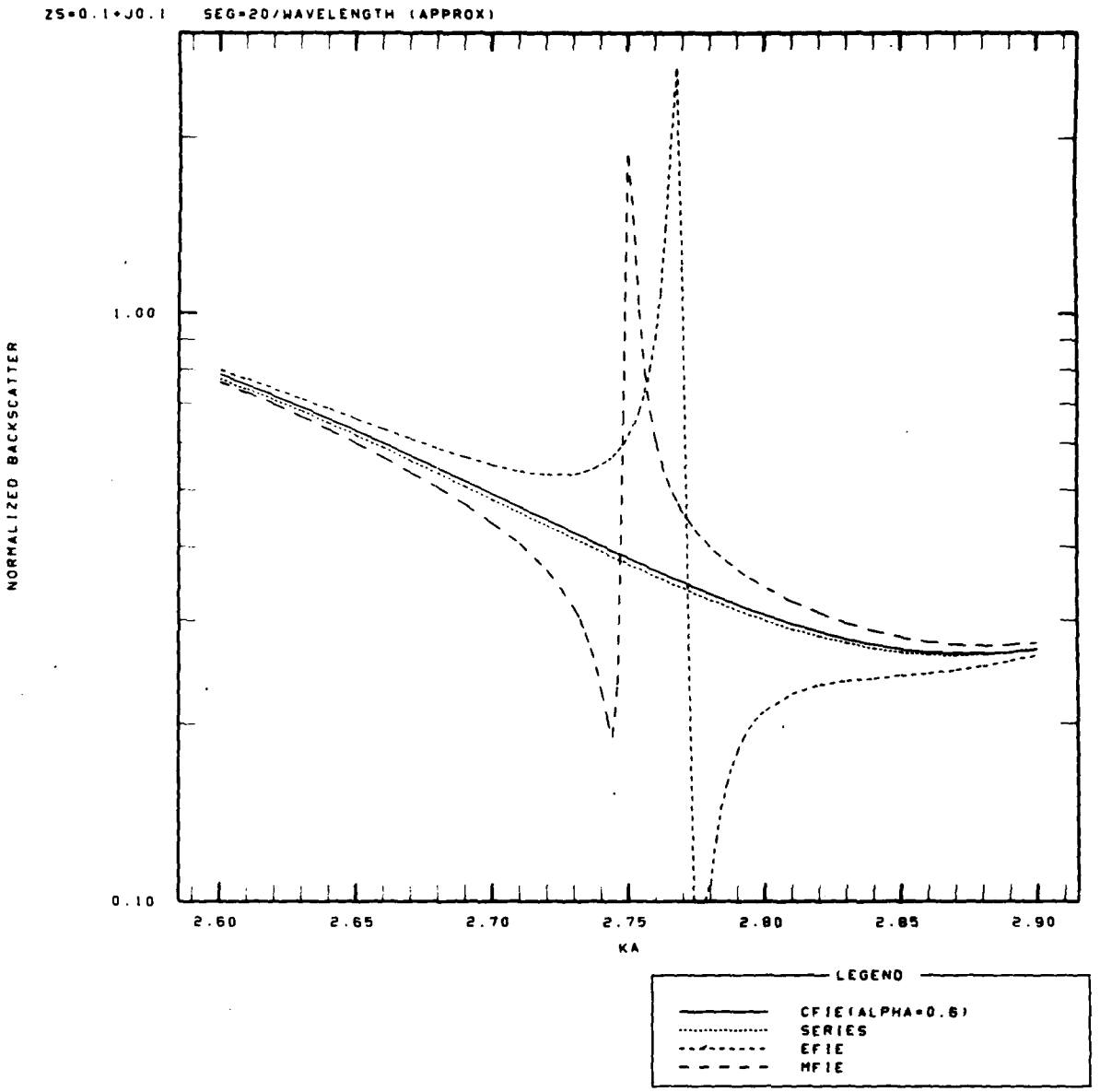

Fig. 4.9a. Normalized backscatter ($\sigma/\pi a^2$) from a lossy impedance sphere having a normalized surface impedance of 0.1 + j0.1 vs. normalized wavenumber (ka).

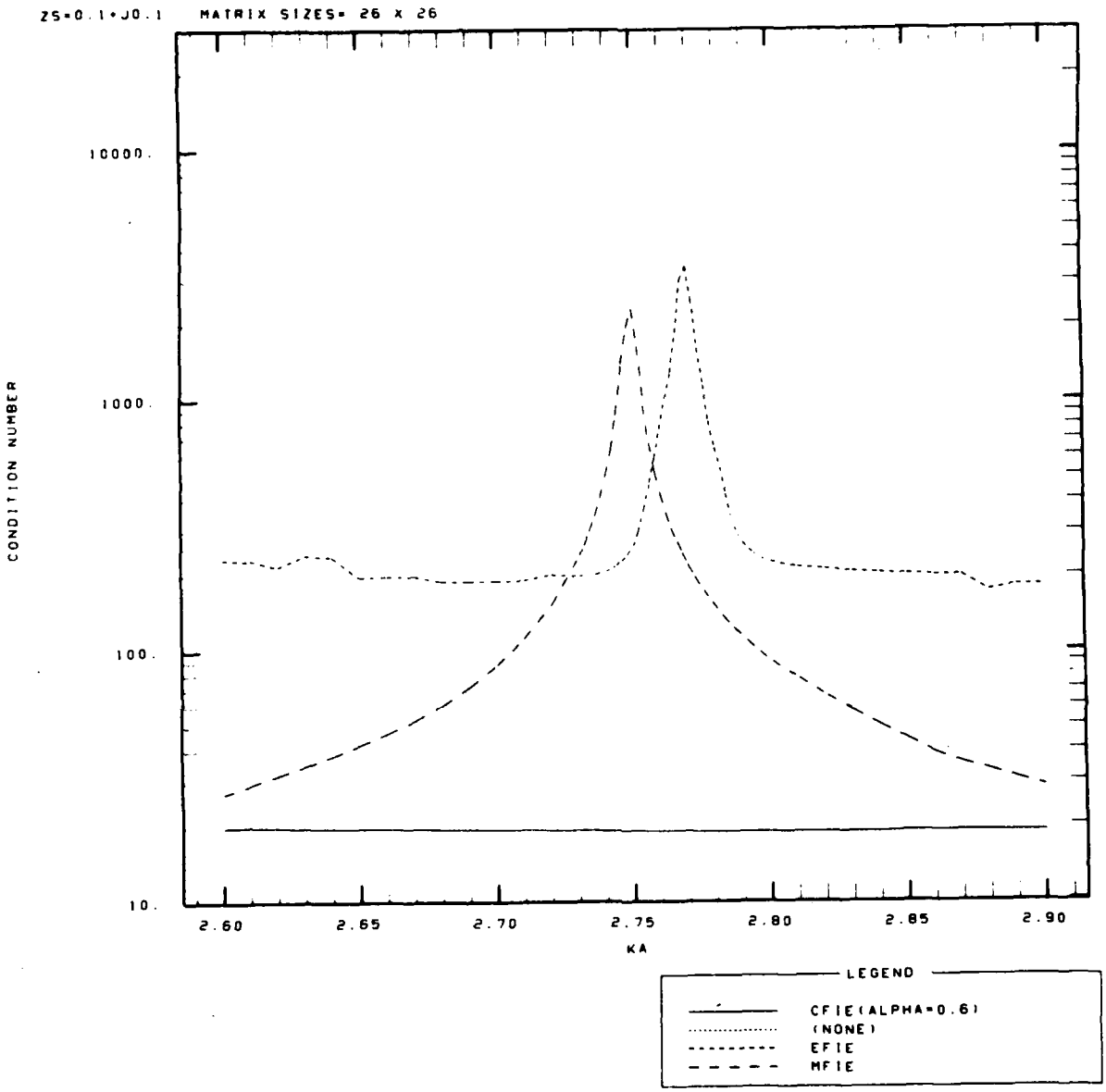

Fig. 4.9b. Matrix condition numbers (m = 1 Fourier mode) for the lossy impedance sphere solutions of Fig. 4.9a vs. ka.

if one assumed that the lossy surface impedance would help regularize the ill-posed equations. Values of condition number, however, are not greatly different from the perfectly conducting case except that the EFIE condition numbers are slightly lower. A possible explanation for these changes in accuracy and stability is offered as follows. As mentioned in the previous section, the non-zero value of Z_s adds a term $(1.0/\eta)\hat{n}xL_H(\vec{M})$ to the perfect conductor EFIE - changing it from a 1st kind equation to a second kind equation. Hence, one would expect that the conditioning of the EFIE for this case should be better than the perfectly conducting case because of the addition of some well-conditioned L_H integral operator to the equation. However, the non-zero Z_s also changes the spurious equivalent currents from the form $(\vec{J},0)$ for the perfectly conducting case to the combined source form $(\vec{J},\vec{M}=-\hat{n}xZ_s\cdot\eta\vec{J})$.[10] These latter currents, which are still equivalent currents of the perfect conductor cavity problem, always have non-zero exterior fields. Thus, the spurious currents of the EFIE radiate an exterior field when Z_s is non-zero and the accuracy in the cross section would be expected to be worse than in the perfect conductor EFIE case. The increased errors in the MFIE cross sections may be due to the combined source spurious equivalent currents producing larger exterior fields than in the perfectly conducting MFIE case.

Effects of a pure real surface impedance on the accuracy and stability of the three integral equations is shown in Fig. 4.10. Normalized backscatter ($\sigma/\pi a^2$) and condition number (cond) are plotted as functions of $Re(Z_s)$ at ka=2.75. $Im(Z_s)$=0.0 and matrix sizes of 26 x 26 are used (SEG=20/λ). Since α=1.0 is the best choice for Z_s=1.0 (as determined in the previous section), this value is used for the CFIE solution at all values of Z_s in Fig. 4.10. At this value of ka (very close to the first theoretical sphere resonance), the EFIE and MFIE are characterized by ill-conditioned matrices and poor accuracy in predicting cross section. In contrast, the CFIE (α=1.0) is relatively well-conditioned and predicts the cross section very close to the Mie series at all values of $Re(Z_s)$. As in the previous case, the lossy surface impedance did not help to regularize the ill-posed integral equation formulations.

The case of Z_s=1.0 appears to be a stressing case in the calculation of scattering from impedance BORs since the theoretical cross section for axial backscattering is zero. Figures 4.11a and b consider this case for a sphere by displaying normalized backscatter ($\sigma/\pi a^2$) vs. ka and cond vs. ka respectively. In Fig. 4.11a, there is a scale change on the vertical axis - the upper scale for the EFIE-MFIE ordinates and the lower scale for the CFIE (α=1.0) ordinates. Since the backscattering predictions of the EFIE and the MFIE are

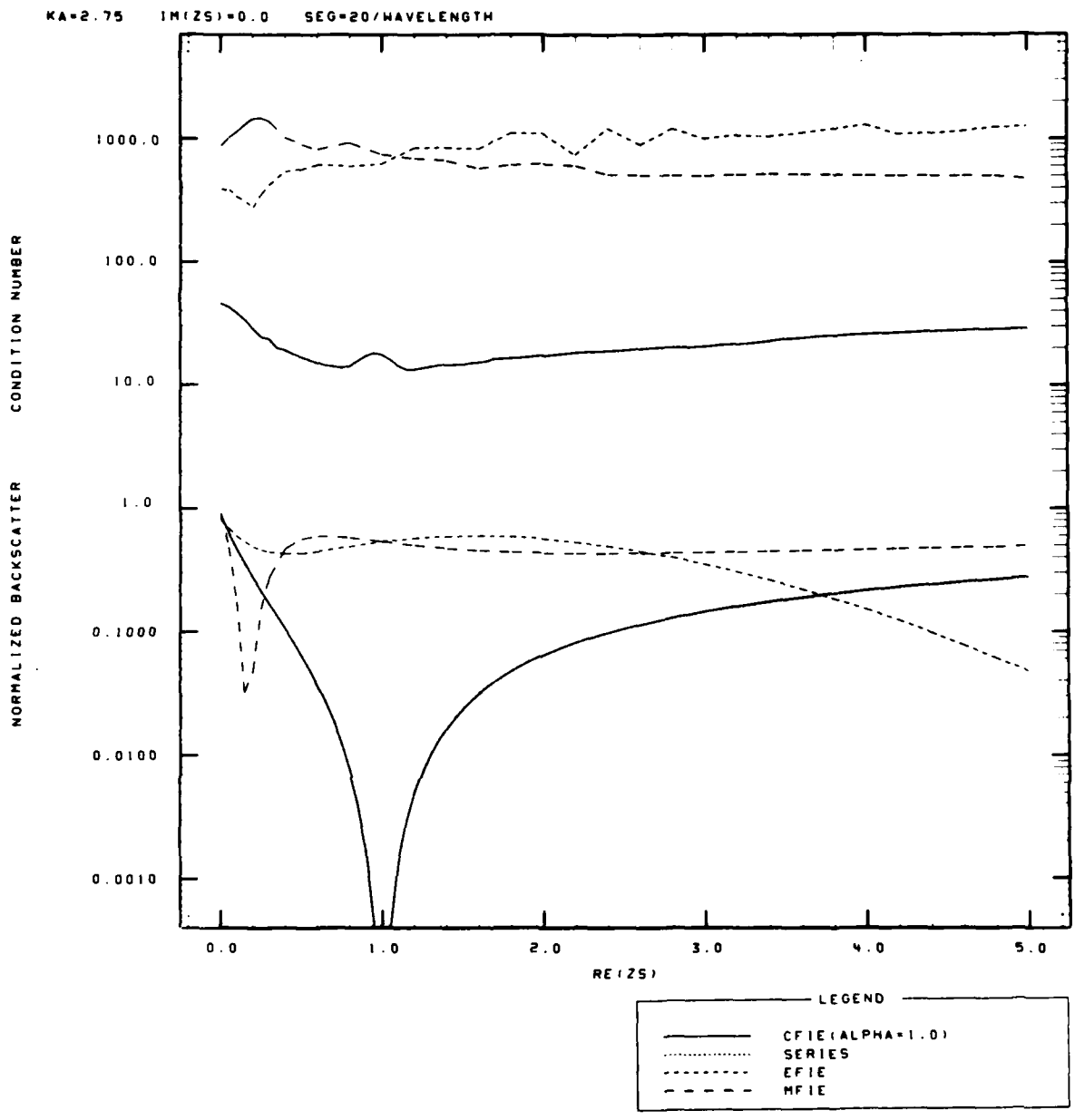

Fig. 4.10. Normalized backscatter (lower set of ordinates) from a lossy impedance sphere and associated matrix condition numbers (upper set of ordinates) vs. real part of normalized surface impedance (imaginary part of Z_s = 0.0, ka = 2.75). Note: the CFIE and Mie series ordinates nearly overlay each other.

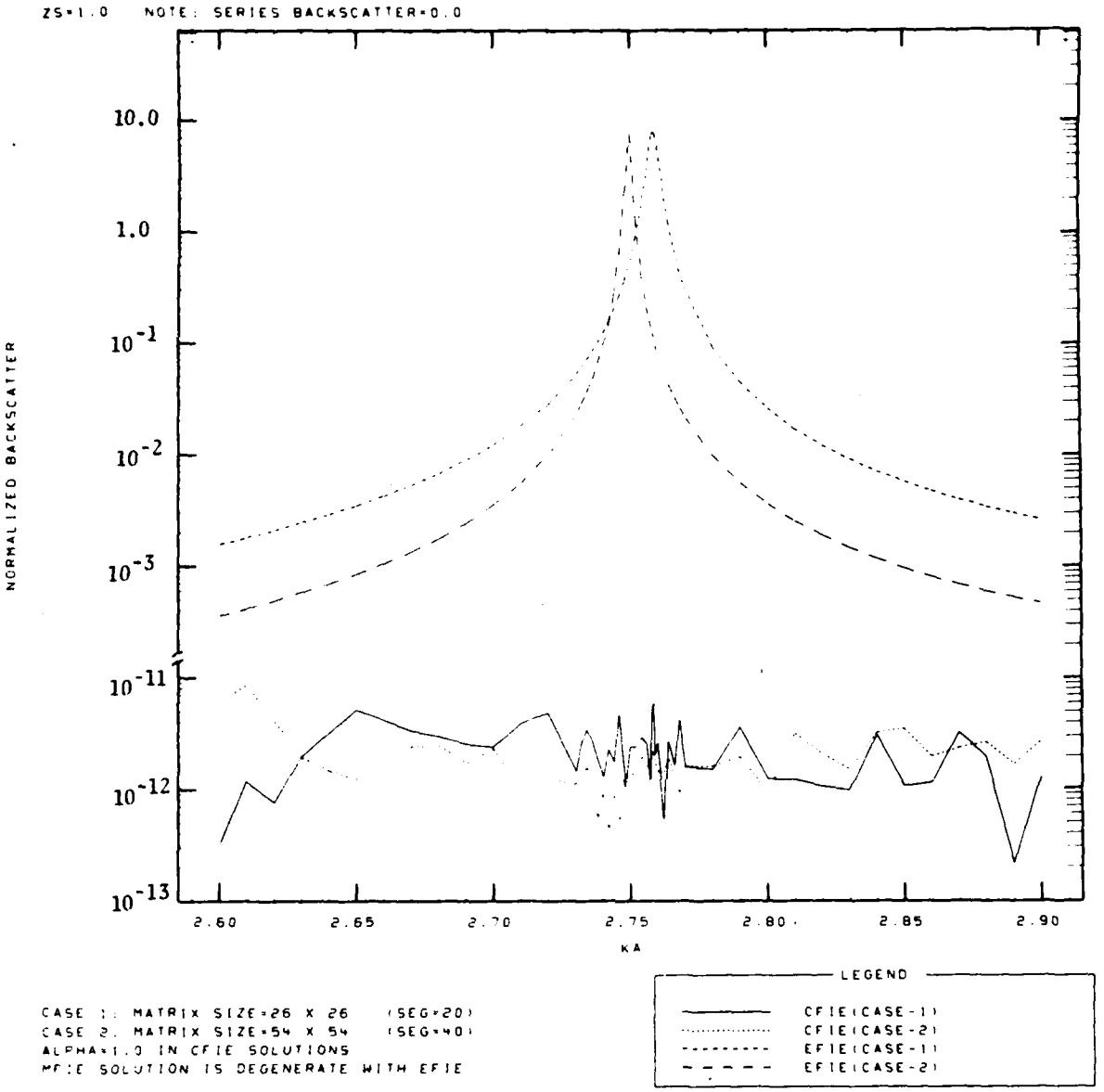

Fig. 4.11a. Normalized backscatter vs. ka for a lossy impedance sphere having normalized surface impedance of 1.0. Note the scale change on the vertical axis. Also, the increased jaggedness of the CFIE ordinates near the center of the figure is due to increased samples in that region.

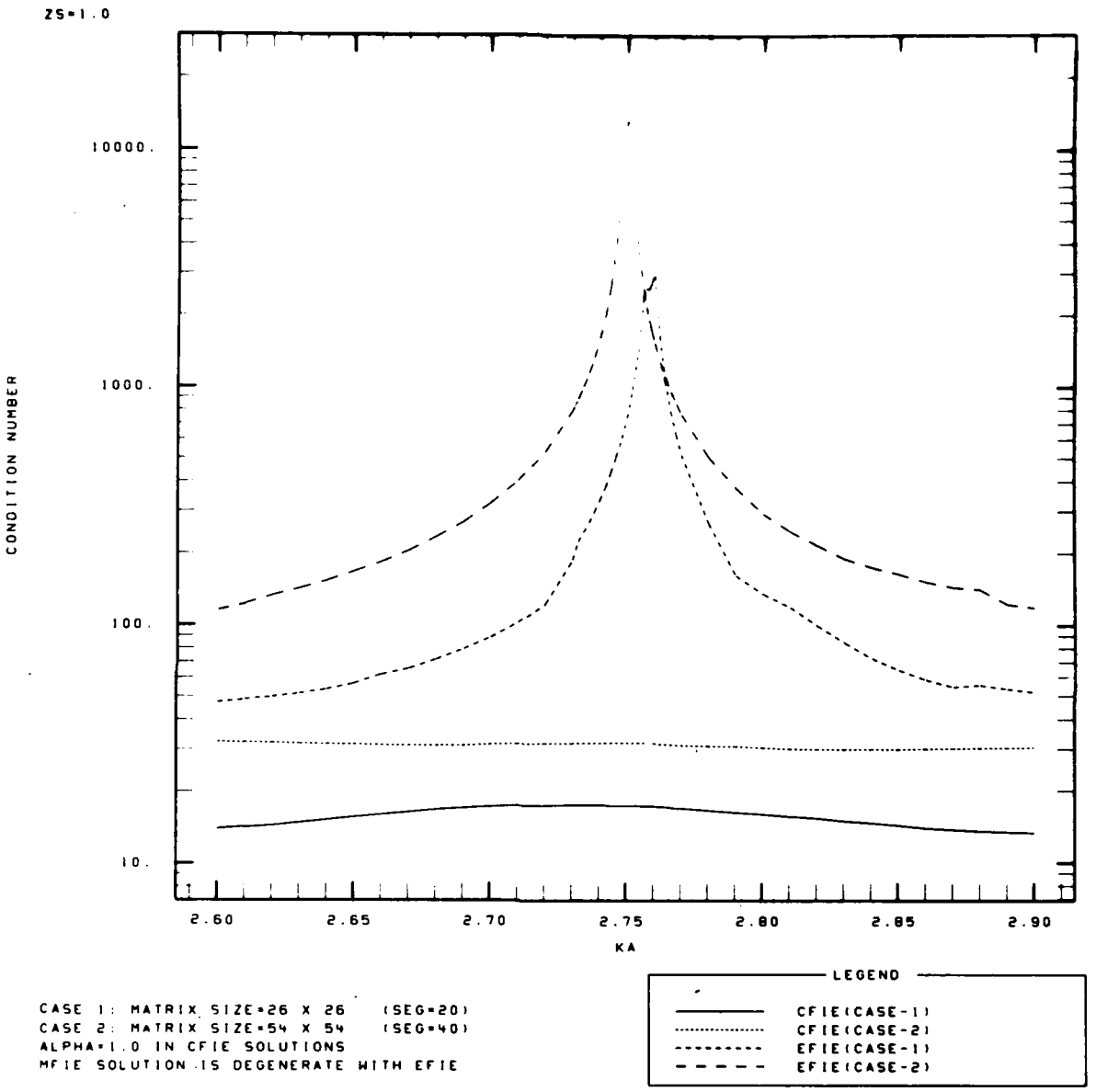

Fig. 4.11b. Matrix condition numbers (m = 1 Fourier mode) vs. ka for the lossy impedance sphere solutions of Fig. 4.11a.

degenerate for Z_s=1.0, there is a common ordinate for both equations. In the figures, two different matrix sizes are used which illustrate the effect of a change in moment-method segmentation upon the influence of the spurious resonance in the impedance sphere scattering solutions with Z_s=1.0. Case 1 corresponds to matrix sizes of 26 x 26 (SEG≈20/λ) and Case 2 corresponds to matrix sizes of 54 x 54 (SEG≈40/λ).

Considering that the exact scattering solution for all ka is zero, the EFIE-MFIE predictions are very poor for all ka values considered in Fig. 4.11a. The cross section values indicated by the EFIE-MFIE ordinates show only the contribution of the spurious equivalent currents to the computed scattered field. The CFIE (α=1.0) predictions, which appear to be computational noise, are a much better approximation to the theoretical cross section. The increase in matrix size upon the EFIE-MFIE solutions has similar effects as those for the perfectly conducting case (Fig. 4.4). Increasing the matrix size causes the bandwidth for errors in cross section to narrow slightly, the scattering predictions to be generally better at a given ka and the predicted location of the resonance to be shifted closer to the theoretical location (ka=2.744). However, increasing the matrix size has little effect on the CFIE (α=1.0) other than an increase in the condition numbers as shown in Fig. 4.11b. A further improvement in the CFIE (α=1.0) cross section predictions

would probably require increasing computational accuracy (which is 32 bit in all numerical examples of this report).

Figures 4.12a, b and c display E-plane bistatic scattering from an impedance sphere having Z_s=1.0 at ka values near the first, second and third perfect conductor sphere resonances respectively. In each case, matrix size is adjusted to obtain SEG=20/λ. Bistatic scattering angles of 0 and 180 degrees correspond to backscattering and forward scattering respectively. The effect of the spurious solutions upon the EFIE and MFIE appears to be similar for each of these resonances - with the predicted location of the resonance being slightly higher than the theoretical location in each case (the ka values of each are very close to the peak of the resonance). In all three cases, the EFIE and MFIE scattering predictions are very poor for all bistatic angles except those near forward scattering. The CFIE (α=1.0) predictions on the other hand, are excellent for all bistatic aspect angles - the curves nearly overlaying the Mie series solutions in all three cases. Although α=1.0 was determined in the previous section to be the best value only at ka=2.75, the excellent agreement of the CFIE (α=1.0) predictions with the Mie series at the other ka values indicates that α=1.0 may be the best value at all frequencies when the normalized surface impedance is 1.0.

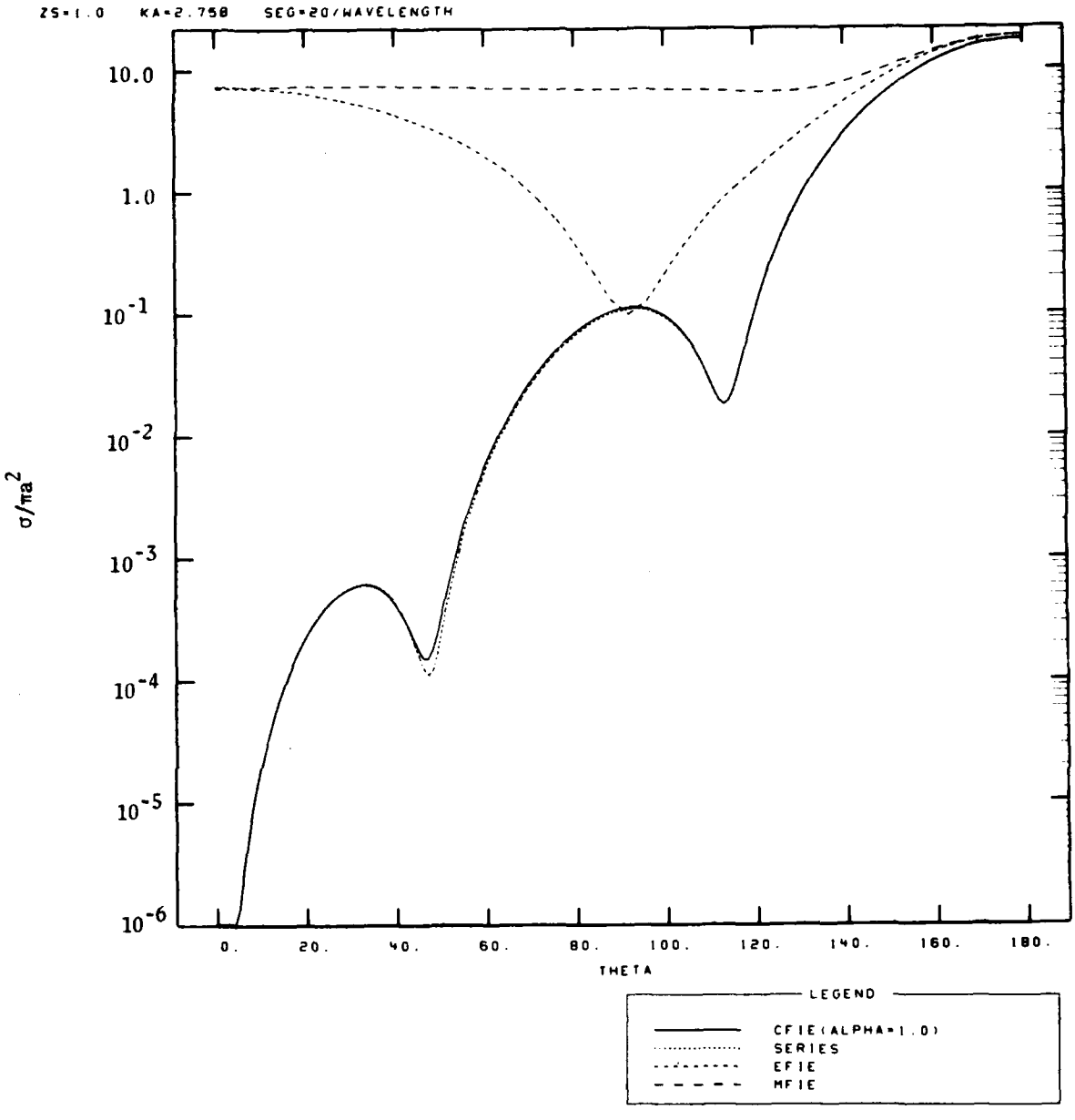

Fig. 4.12a. Normalized E-plane bistatic scattering from a lossy impedance sphere (Z_s = 1.0, ka = 2.758). For the H-plane, interchange the EFIE and MFIE predictions (the CFIE and Mie series predictions for the H-plane are the same as those for the E-plane when Z_s = 1.0).

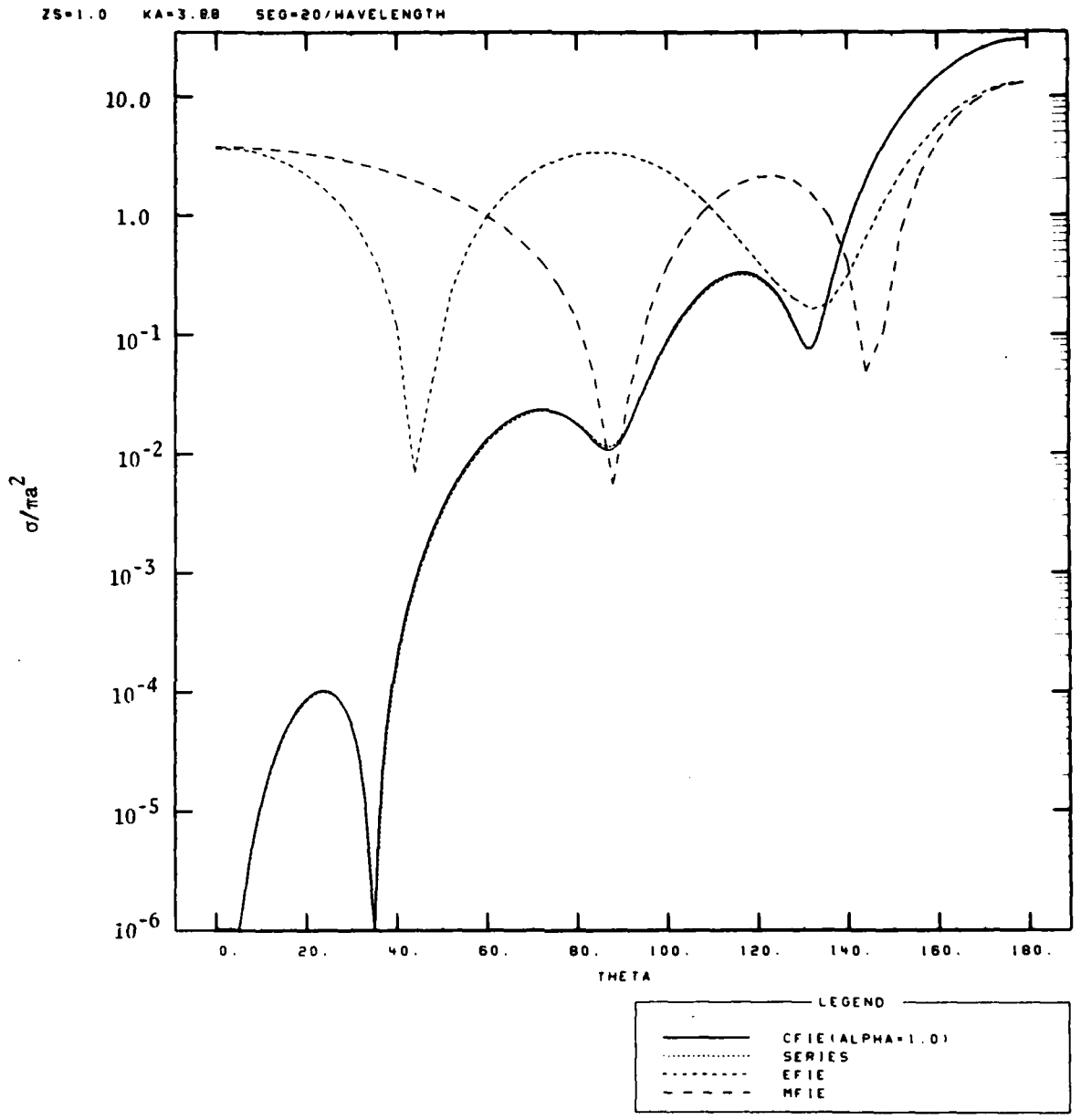

Fig. 4.12b. Normalized E-plane bistatic scattering from a lossy impedance sphere (Z_s = 1.0, ka = 3.88).

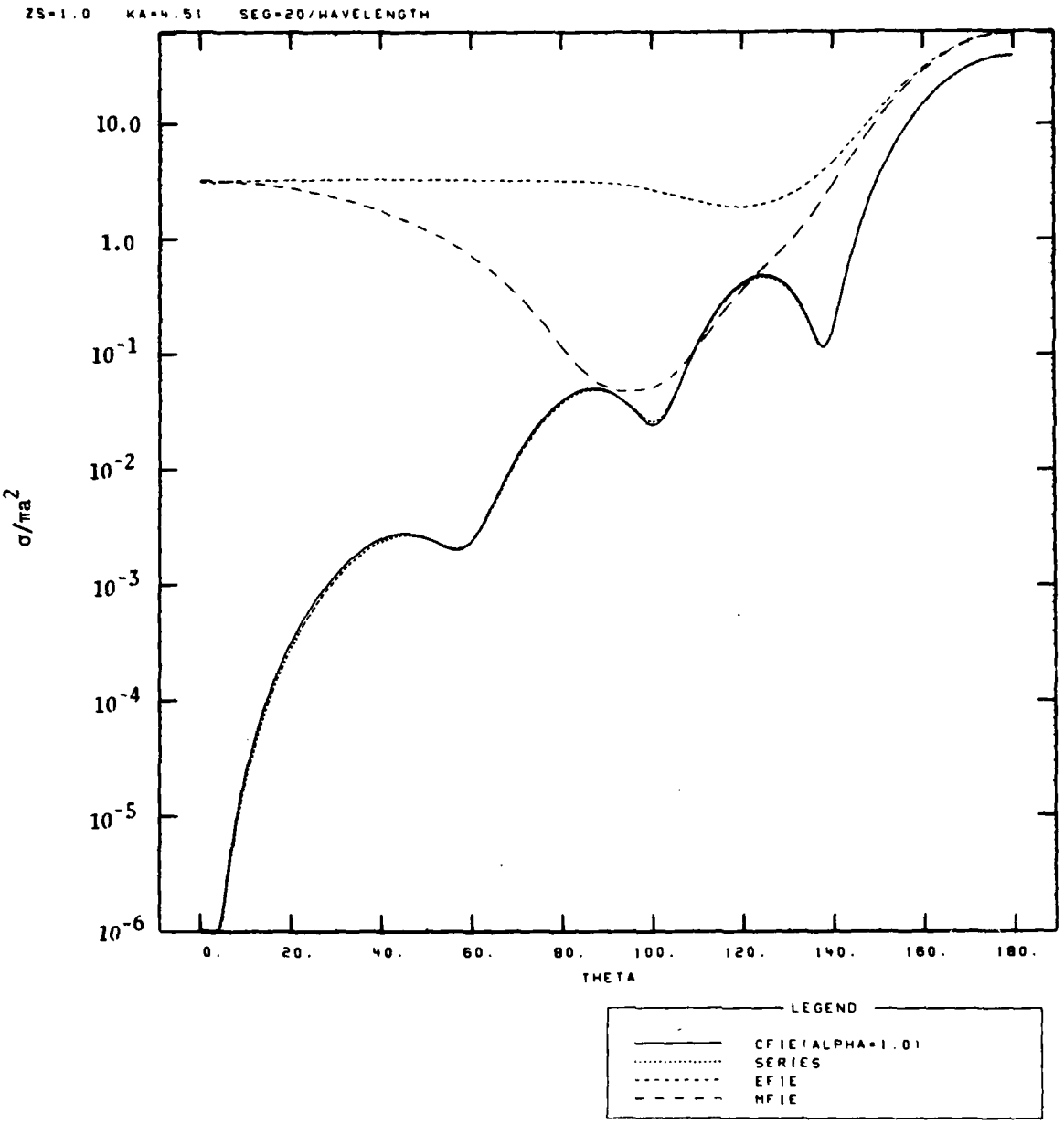

Fig. 4.12c. Normalized E-plane bistatic scattering from a lossy impedance sphere (Z_s = 1.0, ka = 4.51).

Figures 4.13 and 4.14 consider scattering from impedance spheres characterized by a pure reactive surface impedance. Figure 4.13 displays normalized backscatter ($\sigma/\pi a^2$) vs. $Im(Z_s)$ at ka=2.75 with $Re(Z_s)=0$. Four different integral equation solutions are compared to the Mie series: EFIE, MFIE, CFIE (α=1.0) and CFIE (variable α). The last case is presented to demonstrate that an improvement (albeit slight) in accuracy can be attained by varying α as Z_s changes. Figure 4.14 displays condition number vs. $Im(Z_s)$ for each of the integral equation solutions of Fig. 4.13. Matrix sizes are 26 x 26 - corresponding to SEG=$20/\lambda$.

The accuracies of the EFIE and the MFIE in predicting backscatter at ka=2.75 are very poor when Z_s is pure imaginary. In contrast, both CFIE solutions have good agreement with the Mie series. The CFIE (variable α) case represents a slight improvement over the constant α case - although there are still large errors in cross section in the regions where cross section changes greatly with a slight change in $Im(Z_s)$. Values of condition number displayed in Fig. 4.14 indicate that the CFIE solutions are generally better conditioned than the EFIE and MFIE solutions. The stability of the integral equation solutions for large inductive Z_s appears to be strikingly different than that for large capacitive values of Z_s. That is, the impedance

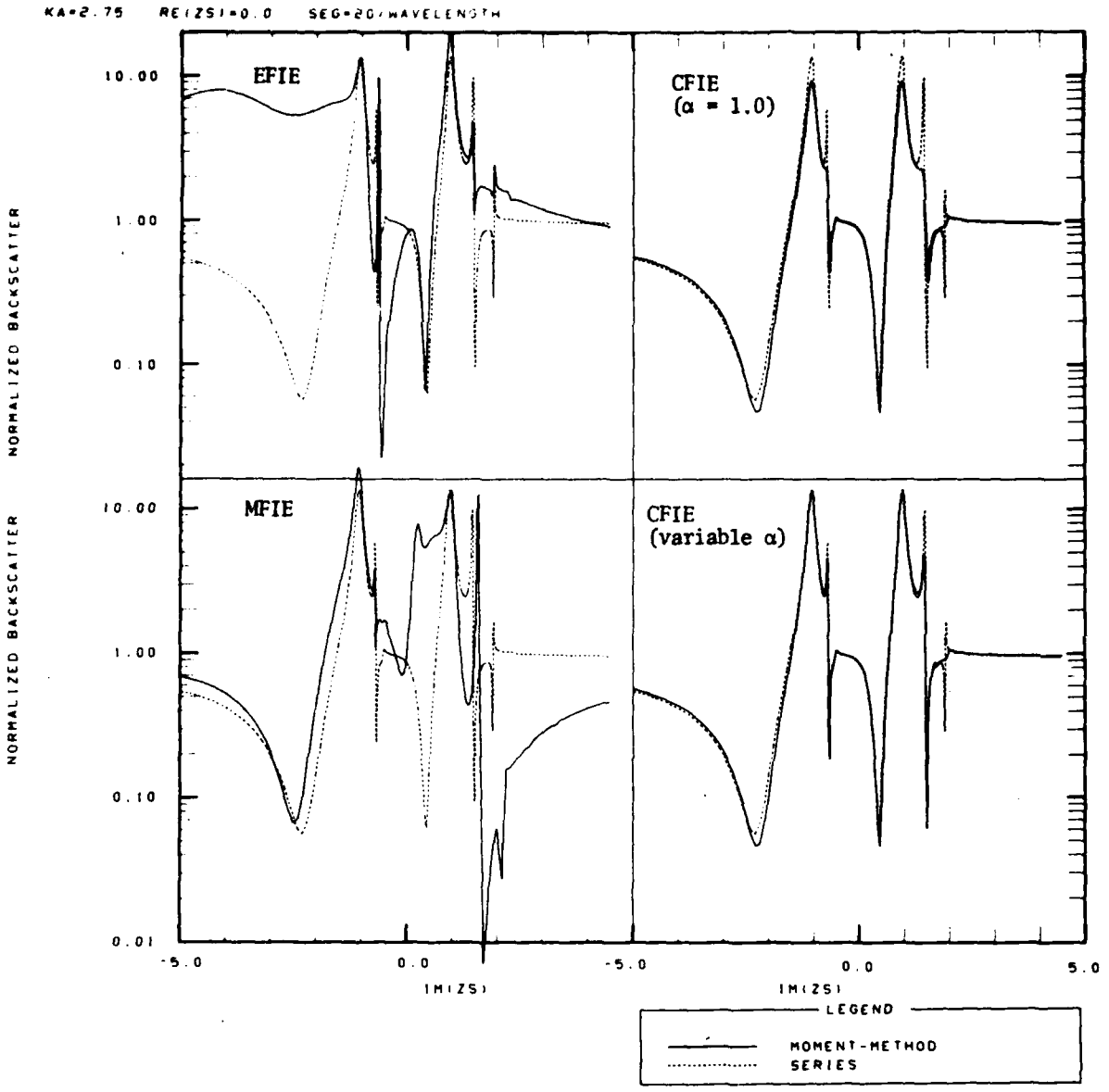

Fig. 4.13. Normalized backscatter from a reactive impedance sphere vs. imaginary part of normalized surface impedance (real part of Z_s = 0.0, ka = 2.75). For the CFIE (variable α) case: $-5.0 < \text{Im}(Z_s) < -1.4$, $\alpha = 1.0$; $-1.4 < \text{Im}(Z_s) < -0.6$, $\alpha = .12$; $-0.6 < \text{Im}(Z_s) < 0.6$, $\alpha = 1.0$; $0.6 < \text{Im}(Z_s) < 1.7$, $\alpha = 8.0$; and $1.7 < \text{Im}(Z_s) < 5.0$, $\alpha = 1.0$.

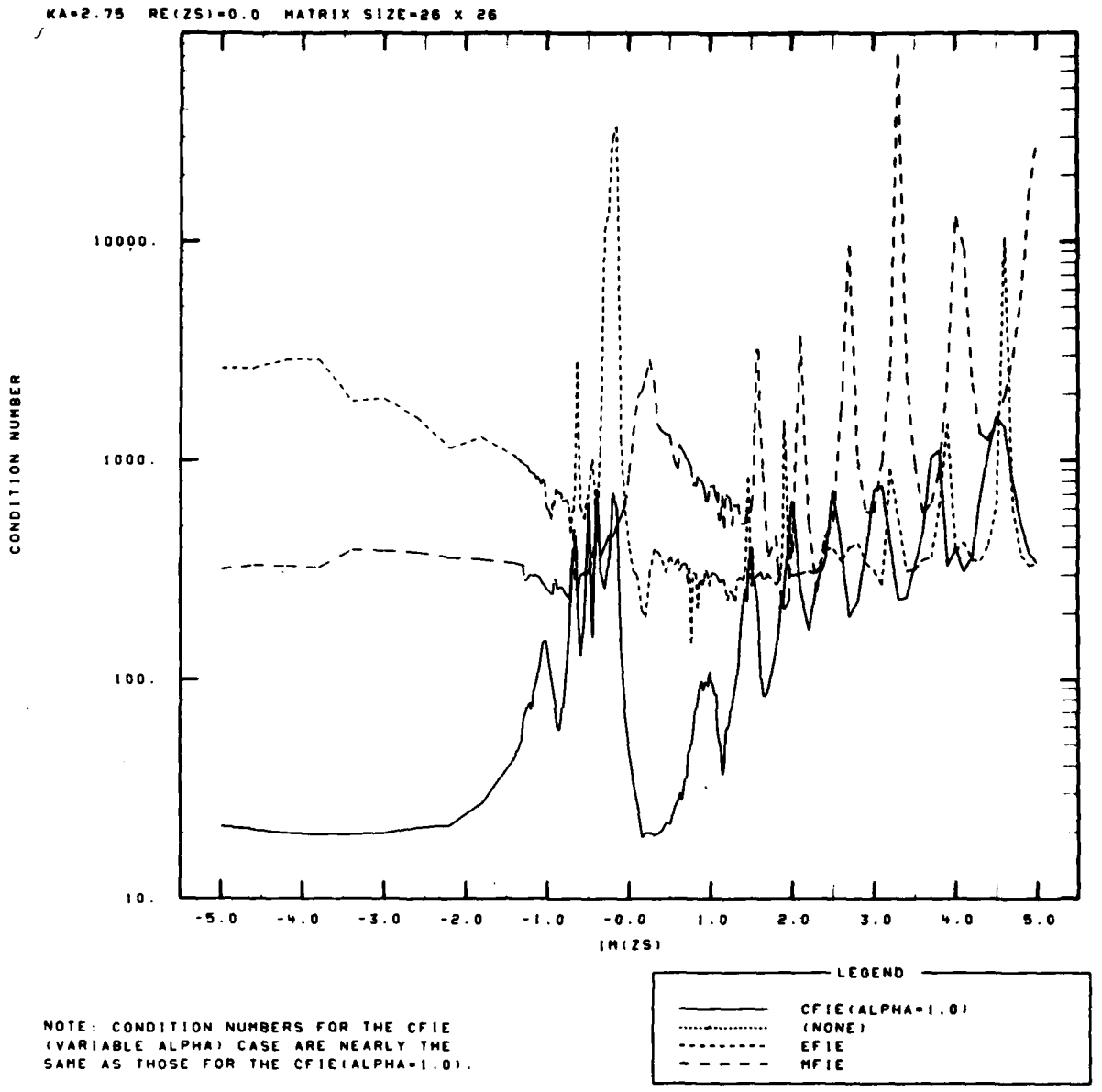

Fig. 4.14. Matrix condition numbers (m = 1 Fourier mode) vs. imaginary part of Z_s for the reactive impedance spheres of Fig. 4.13.

spheres appear to be characterized by resonances for large inductive Z_s - possibly exterior surface wave resonances. This behavior is similar to that noted by Wait in Mie series solutions of scattering from impedance spheres.[14]

5.0 CONCLUSIONS

This report has investigated numerical solutions to integral equation formulations for scattering from bodies described by a Leontovich impedance boundary condition (IBC). A method of constructing moment-method solutions to three different IBC integral equations was described. Two of these equations - the principal ones for which numerical solutions have been obtained - are the electric and magnetic field integral equations (EFIE and MFIE). These two equations are ill-posed because they theoretically allow spurious solutions at frequencies at interior perfect conductor cavity resonances. The IBC combined field integral equation (CFIE) - which has received little attention in terms of actual numerical solutions - is well-posed because it rejects the spurious resonances. Numerical solutions to the EFIE, MFIE and CFIE for scattering from impedance spheres were presented in this report which considered different types of impedance surfaces (i.e., perfectly conducting, lossy, reactive, etc.)

The numerical results demonstrated that scattering solutions to the EFIE and MFIE can be severely contaminated by spurious solutions when at a frequency near an interior resonance. This contamination occurs regardless of whether the surface impedance is lossy or lossless and no regularization of the ill-posedness of these equations occurs when the surface impedance is lossy. In

contrast to the MFIE and the EFIE, solutions to the CFIE are not affected by spurious resonant solutions when a suitable choice of integral equation weighting coefficient (α) can be determined. The CFIE solutions are consistently more stable and accurate than those of the EFIE or the MFIE when at a frequency near an interior resonance. For some values of Z_s (for example Z_s=1.0) the solution accuracy of the CFIE can be much better than that of the EFIE or MFIE even when at a frequency that appears to be far from an interior resonance. Thus, the numerical examples clearly demonstrated that the CFIE is in practice (as in theory) a superior IBC integral equation formulation to either the EFIE or the MFIE.

The numerical examples also illustrated some important differences when the scatterer surface has a non-zero surface impedance than when the scatterer is a perfect conductor (this latter case being the one upon which current understanding of the effects of spurious solutions on an integral equation formulation is based). First, when Z_s is non-zero, relative errors in the computed EFIE and MFIE cross sections are generally larger and the bandwidths for errors are generally wider than those for the perfect conductor EFIE and MFIE. This appears to be due to the fact that when Z_s is non-zero, the spurious equivalent currents take the combined source form $(\hat{J},\hat{M}=-\hat{n}x\hat{Z}_s\cdot\eta\hat{J})$ rather than the form $(\hat{J},0)$. The combined source equivalent currents (which are

still equivalent currents of the perfect conductor interior resonance problem) radiate an exterior electromagnetic field which depends in magnitude upon the value of Z_s. Thus, the use of a well-posed integral equation formulation takes on greater importance when the scatterer surface impedance is non-zero than for the perfect conductor case. Secondly, when Z_s is non-zero, choice of moment- method segmentation (SEG) and integral equation weighting coefficient (α) for the CFIE appears to be more complicated to attain a specified cross section accuracy than the perfect conductor case. Convergence as a function of SEG appears to be very poor for certain values of reactive surface impedance (low loss) at certain frequencies. In particular, when the frequency is near an exterior surface wave resonance (where there might be a very large cross section or one that changes rapidly with frequency), the errors may be large regardless of segmentation. When varying α at a given SEG, the best accuracy of the CFIE occurs at different values of α for different values of Z_s. Thus, the established perfect conductor criteria for choosing α is not adequate for all Z_s.

APPENDIX A

The Fortran IV computer program listed in this appendix is essentially Mautz and Harrington's main program[13] for the perfect conductor case extended to the impedance boundary condition case. Several variables (ZS, ZST, ZSP, YY, ZZ, TM, PM) and one subroutine (MATB) were added to accomplish the required modifications. Also, many comments were added to aid in understanding the logic of the program and all the main variables. Some minor changes to Mautz and Harrington's program were that the inputs were changed to list-directed read and all format statements for outputs were moved to the end of the program. The output was modified to include printing of the two components of magnetic surface current density (sampled at the same body locations as the electric surface current density). The listing does not include any routines from the Mautz and Harrington program that are unchanged.

Solution is obtained for the following conditions: (1) single excitation frequency, (2) one incident angle and one scattering angle (not necessarily the same), and (3) one value of normalized surface impedance on the BOR. The actual program used for generating the results of Chapter 4 was a modification of the one listed in this appendix which could calculate scattering at many aspect angles, frequencies, etc. (by appropriate insertion of loops).

```
C   PROGRAM IBC - THIS PROGRAM SOLVES FOR THE ELECTROMAGNETIC
C      SCATTERING FROM A BODY OF REVOLUTION HAVING A SURFACE
C      CHARACTERIZED BY A LEONTOVICH IMPEDANCE BOUNDARY CONDITION
C      (IBC).  A MOMENT-METHOD SOLUTION IS OBTAINED FROM THE
C      ELECTRIC FIELD INTEGRAL EQUATION (EFIE), THE MAGNETIC
C      FIELD INTEGRAL EQUATION (MFIE) AND THE COMBINED FIELD
C      INTEGRAL EQUATION (CFIE).  THE INTERNAL CODING OF THE
C      PROGRAM ASSUMES A NORMALIZED, DIAGONAL, DYADIC SURFACE
C      IMPEDANCE WHICH CAN HAVE ARBITRARY VARIATIONS ALONG THE
C      LONGITUDINAL SURFACE COORDINATE OF THE BOR.  HOWEVER, THIS
C      VERSION READS IN A SCALAR, CONSTANT VALUE OF NORMALIZED
C      SURFACE IMPEDANCE.
C
C      THIS PROGRAM IS A GENERALIZATION MAUTZ AND HARRINGTON'S
C      MOMENT-METHOD PROGRAMS FOR SCATTERING FROM A PERFECTLY
C      CONDUCTING (P.C.) BOR.  DETAILS OF THE MOMENT-METHOD AND
C      REQUIRED (BUT UNMODIFIED) SUBROUTINES ARE DOCUMENTED IN:
C
C      1.  J. R. MAUTZ AND R. F. HARRINGTON, 'H-FIELD, E-FIELD,
C      AND COMBINED FIELD SOLUTIONS FOR BODIES OF REVOLUTION',
C      TECHNICAL REPORT TR-77-2, (FEBRUARY 1977), AND
C      'COMPUTER PROGRAMS FOR H-FIELD, E-FIELD, AND COMBINED
C      FIELD SOLUTIONS FOR BODIES OF REVOLUTION', TR-77-3, (MAY
C      1977), DEPARTMENT OF ELECTRICAL AND COMPUTER ENGINEERING,
C      SYRACUSE UNIVERSITY, SYRACUSE, NY 13210
C
C      THE BOR SURFACE IS DESCRIBED BY A LONGITUDINAL COORDINATE
C      T AND AN AZIMUTHAL COORDINATE PHI.  THE FAR FIELD POINTS
C      ARE DESCRIBED BY THETA AND PHI SPHERICAL COORDINATES.  ALL
C      SURFACE VECTORS AND DYADICS USE THE BODY COORDINATE SYSTEM
C      WHILE THE VARIOUS LINEAR POLARIZATIONS OF THE INCIDENT AND
C      SCATTERED WAVES REFER TO THE SPHERICAL COORDINATE SYSTEM.
C
C   ROUTINES CALLED:
C      MATB  - CONSTRUCTS PART OF THE IMPEDANCE OR ADMITTANCE
C              MATRICES FOR THE IBC EQUATIONS FROM THE PERFECT
C              CONDUCTOR MATRICES.
C      YZ    - CALCULATES THE PERFECT CONDUCTOR IMPEDANCE AND
C              ADMITTANCE MATRICES (SEE REFERENCE 1)
C      PLANE - COMPUTES MEASUREMENT MATRICES FOR THE TRANSMITTER
C              AND RECEIVER ANGLES (SEE REFERENCE 1)
C      DECOMP- COMPUTES THE MATRIX DECOMPOSITION OF THE IMPEDANCE
C              OR ADMITTANCE MATRICES (SEE REFERENCE 1)
C      SOLVE - SOLVES THE LINEAR SYSTEM OF ALGEBRAIC EQUATIONS
C              FOR A GIVEN SOURCE VECTOR (SEE REFERENCE 1)
C
C   FILE DEFINITIONS: 5 - INPUT FILE (ALL INPUTS FREE FORMAT)
C                     6 - OUTPUT FILE
```

```
C
C   INPUT VARIABLES:
C      NM   - TOTAL NUMBER OF FOURIER MODES (0,1,2,...,NM-1)
C      NP   - NUMBER OF PROFILE BODY POINTS (ODD NUMBER, G.E. 5)
C      NPHI - NUMBER OF POINTS IN GAUSSIAN QUADRATURE INTEGRATION
C      BK   - WAVENUMBER (UNITS CONSISTENT WITH RH AND ZH)
C      TT   - TRANSMITTER THETA ANGLE (DEGREES)
C             (NOTE:  TRANSMITTER PHI ANGLE = 0.0)
C      P    - BODY PHI ANGLE (DEGREES) IDENTIFYING THE PLANE IN
C             WHICH THE SURFACE CURRENT DENSITIES ARE EVALUATED.
C      TR   - RECEIVER THETA ANGLE (DEGREES)
C      PR   - RECEIVER PHI ANGLE (DEGREES)
C      ALP  - INTEGRAL EQUATION WEIGHTING COEFFICIENT
C      RH   - P CYLINDRICAL COORDINATE OF BODY POINTS
C      ZH   - Z CYLINDRICAL COORDINATE OF BODY POINTS
C      X    - ABSCISSAS OF GAUSSIAN QUADRATURE INTEGRATION
C      A    - WEIGHTS OF GAUSSIAN QUADRATURE INTEGRATIONS
C      ZS   - NORMALIZED SURFACE IMPEDANCE (SCALAR, CONSTANT)
C
C   OTHER MAIN VARIABLES:
C      N    - NUMBER OF EXPANSION FUNCTIONS
C      N2   - MATRIX DIMENSION
C      ZST  - T-T COMPONENT, NORMALIZED DYADIC SURFACE IMPEDANCE
C      ZSP  - PHI-PHI COMPONENT, NORM. DYADIC SURFACE IMPEDANCE
C      Y    - NORMALIZED ADMITTANCE MATRIX FOR THE P.C. MFIE
C      Z    - NORMALIZED IMPEDANCE MATRIX FOR P.C. EFIE
C      YY   - NORMALIZED ADMITTANCE MATRIX FOR IBC MFIE
C      ZZ   - NORMALIZED IMPEDANCE MATRIX FOR IBC EFIE
C      RT   - MEASUREMENT MATRIX FOR TRANSMITTER THETA ANGLE
C      RR   - MEASUREMENT MATRIX FOR RECEIVER THETA ANGLE
C      B    - SOURCE VECTOR (FROM INCIDENT FIELDS)
C      C    - SOLUTION VECTOR
C      KT   - DENOTES TRANSMITTER POLARIZATION (1=THETA, 2=PHI)
C      KR   - DENOTES RECEIVER POLARIZATION (1=THETA, 2=PHI)
C      NHEC - DENOTES TYPE EQUATION (1=MFIE, 2=EFIE, 3=CFIE)
C      TJ   - T-COMPONENT OF NORMALIZED ELECTRIC SURFACE CURRENT
C      PJ   - PHI-COMPONENT OF NORM. ELECTRIC SURFACE CURRENT
C      TM   - T-COMPONENT OF NORMALIZED MAGNETIC SURFACE CURRENT
C      PM   - PHI-COMPONENT OF NORM. MAGNETIC SURFACE CURRENT
C      E    - NORMALIZED RCS (SIGMA/LAMBDA**2)
C
C   OUTPUTS:
C      1.  ALL INPUT PARAMETERS
C      2.  SAMPLE OUTPUT OF THE EFIE, MFIE AND CFIE MATRICES,
C          AND SAMPLE OUTPUT FROM PLANE, DECOMP AND SOLVE.
C      3.  FOR EACH INTEGRAL EQUATION AND EACH TRANSMITTER
C          POLARIZATION, THE FOLLOWING ARE PRINTED:
C          A.  TJ, PJ, TM, PM  AT N DISCRETE LOCATIONS ALONG THE
```

```
C              T COORDINATE (MEASURED IN THE PHI=P PLANE)
C          5.  NORMALIZED RCS FOR BOTH RECEIVER POLS.
C
C   THE MEANING OF 'NORMALIZED' IS AS FOLLOWS.  THE IMPEDANCE
C      (ADMITTANCE) MATRICES AND THE SURFACE IMPEDANCE ARE
C      NORMALIZED BY DIVISION (MULTIPLICATION) WITH THE FREE
C      SPACE WAVE IMPEDANCE.  THE ELECTRIC AND MAGNETIC SURFACE
C      CURRENT DENSITY COMPONENTS ARE NORMALIZED BY DIVISION WITH
C      THE WAVENUMBER.  IN THE PROGRAM, RH AND ZH ARE NORMALIZED
C      BY MULTIPLICATION WITH THE WAVENUMBER.  THE RCS IS
C      NORMALIZED BY DIVISION OF A SQUARE WAVELENGTH.
C
C   THIS VERSION WAS WRITTEN BY J. ROGERS OF THE RADAR SYSTEMS
C      GROUP, MIT LINCOLN LABORATORY, LEXINGTON, MASS. 02173
C      NOVEMBER 1983.
C
C   DISCLAIMER:  THIS PROGRAM IS EXPERIMENTAL AND WAS WRITTEN TO
C      ILLUSTRATE CERTAIN PROPERTIES OF IBC INTEGRAL EQUATIONS.
C      NO EFFORT WAS MADE TO OPTIMIZE COMPUTER SPEED OR STORAGE.
C      THE BASIC CODING CAN BE VALIDATED FOR THE P.C. CASE BY
C      COMPARING TO THE SAMPLE PROBLEM OF REFERENCE 1.  FOR THE
C      IBC CASE, CHECKS CAN BE MADE WITH THE NUMERICAL EXAMPLES
C      OF THE TECHNICAL REPORT FOR WHICH THIS LISTING IS PART OF.
C
      COMPLEX U,TJ(120),PJ(120),E(12),SN,SNR,RT(240),RR(240)
      COMPLEX Y(1600),Z(1600),B(40),C(40),U1,CONJG
      COMPLEX TM(120),PM(120),YY(1600),ZZ(1600)
      COMPLEX ZS,ZST(20),ZSP(20)
      DIMENSION RH(43),ZH(43),X(20),A(20),THT(3),THR(3),R2(20)
      DIMENSION IPS(40)
C
      READ(5,*) NM,NP,NPHI
      READ(5,*) BK,TT,P,TR,PR,ALP
      READ(5,*) (RH(I),I=1,NP)
      READ(5,*) (ZH(I),I=1,NP)
      READ(5,*) (X(K),K=1,NPHI)
      READ(5,*) (A(K),K=1,NPHI)
      READ(5,*) ZS
C
      WRITE(6,49) NM,NP,NPHI
      WRITE(6,48) BK,TT,P,TR,PR,ALP
      WRITE(6,45) (RH(I),I=1,NP)
      WRITE(6,44) (ZH(I),I=1,NP)
      WRITE(6,47) (X(K),K=1,NPHI)
      WRITE(6,43) (A(K),K=1,NPHI)
      WRITE(6,100) ZS
C
      N2=NP-3
```

```
      N=N2/2
      N3=N2+N
      N4=N2*N2
      N6=6*N
      U=(0.,1.)
      PI=3.141592653
      P4=.0625/PI**3
      P8=PI/180.
      ETA=120.0*PI
      THT(1)=TT*P8
      P=P*P8
      THR(1)=TR*P8
      PR=PR*P8
C
      DO 101 I=1,N
      ZSP(I)=ZS
      ZST(I)=ZS
  101 CONTINUE
      DO 42 J=1,NP
      RH(J)=BK*RH(J)
      ZH(J)=BK*ZH(J)
   42 CONTINUE
      DO 17 J=1,N
      R2(J)=1./RH(2*J+1)
   17 CONTINUE
      DO 54 J=1,N6
      TJ(J)=0.
      PJ(J)=0.
      TM(J)=0.
      PM(J)=0.
   54 CONTINUE
      DO 55 J=1,12
      E(J)=0.
   55 CONTINUE
      WRITE(6,9)
C                                  LOOP THROUGH ALL FOURIER MODES
      DO 41 K=1,NM
      NN=K-1
      PN=NN*P
      CS=COS(PN)
      SN=2.*SIN(PN)*U
      PN=NN*PR
      CSR=COS(PN)
      SNR=2.*SIN(PN)*U
      IF(NN.EQ.0)GO TO 56
      CS=2.0*CS
      CSR=2.0*CSR
   56 LANE=0
```

```
C                                       CALCULATE YY AND ZZ FOR THIS MODE
      CALL YZ(NN,NP,NPHI,RH,ZH,X,A,Y,Z)
      DO 130 I=1,N4
         YY(I)=Y(I)
         ZZ(I)=Z(I)
  130 CONTINUE
      CALL MATB(N2,ZSP,ZST,Z)
      CALL MATB(N2,ZSP,ZST,Y)
      DO 131 I=1,N4
         YY(I)=YY(I)+Z(I)
         ZZ(I)=ZZ(I)+Y(I)
  131 CONTINUE
C                                       LOOP THROUGH THE THREE IBC EQ'S
      DO 58 NHEC=1,3
      GO TO (61,62,63),NHEC
   61 DO 105 JJ=1,N4
         Y(JJ)=YY(JJ)
  105 CONTINUE
      WRITE(6,8)Y(1),Y(2)
      GO TO 59
   62 DO 103 JJ=1,N4
         Y(JJ)=ZZ(JJ)
  103 CONTINUE
      WRITE(6,8)Y(1),Y(2)
      GO TO 59
   63 WRITE(6,8)YY(1),YY(2),ZZ(1),ZZ(2)
      DO 66 J=1,N4
      Y(J)=YY(J)+ALP*ZZ(J)
   66 CONTINUE
C                                       CALCULATE MATRIX DECOMPOSITION
   59 CALL DECOMP(N2,IPS,Y)
      WRITE(6,8)Y(1),Y(2)
      IF(LANE.NE.0)GO TO 57
      LANE=1
C                                       CALCULATE MEASUREMENT MATRICES
      CALL PLANE(NN,N,1,THT,RT)
      CALL PLANE(NN,N,1,THR,RR)
      WRITE(6,8)RT(1),RT(2),RR(1),RR(2)
C                                       CALCULATE SOURCE VECTORS
   57 DO 27 KT=1,2
      L=2*(NHEC-1)+KT
      GO TO (31,32,33,34,35,36),L
C                                       MFIE - THETA TRANSMITTER POL.
   31 DO 21 J=1,N
      B(J)=-RT(J+N3)
      B(J+N)=-RT(J+N2)
   21 CONTINUE
      GO TO 53
```

```
C                                       MFIE - PHI POL.
   32 DO 22 J=1,N
      JN=J+N
      B(J)=-RT(JN)
      B(JN)=-RT(J)
   22 CONTINUE
      GO TO 53
C                                       EFIE - THETA POL.
   33 DO 23 J=1,N
      B(J)=RT(J)
      JN=J+N
      B(JN)=-RT(JN)
   23 CONTINUE
      GO TO 53
C                                       EFIE - PHI POL.
   34 DO 24 J=1,N
      B(J)=-RT(J+N2)
      B(J+N)=RT(J+N3)
   24 CONTINUE
      GO TO 53
C                                       CFIE - THETA POL.
   35 DO 25 J=1,N
      B(J)=-RT(J+N3)+ALP*RT(J)
      JN=J+N
      B(JN)=-RT(J+N2)-ALP*RT(JN)
   25 CONTINUE
      GO TO 53
C                                       CFIE - PHI POL.
   36 DO 26 J=1,N
      JN=J+N
      B(J)=-RT(JN)-ALP*RT(J+N2)
      B(JN)=-RT(J)+ALP*RT(J+N3)
   26 CONTINUE
C                                       SOLVE MATRIX EQUATION
   53 CALL SOLVE(N2,IPS,Y,B,C)
      WRITE(6,8)C(1),C(2)
C                                       CALCULATE NORMALIZED ELECTRIC
C                                       SURFACE CURRENT DENSITY
      J1=(L-1)*N
      GO TO (11,12),KT
   11 DO 13 J=1,N
      J2=J+J1
      TJ(J2)=TJ(J2)+C(J)*CS
      PJ(J2)=PJ(J2)+C(J+N)*SN
   13 CONTINUE
      GO TO 14
   12 DO 15 J=1,N
      J2=J+J1
```

```
      TJ(J2)=TJ(J2)+C(J)*SN
      PJ(J2)=PJ(J2)+C(J+N)*CS
   15 CONTINUE
C                                     CALCULATE NORMALIZED RCS
   14 DO 16 KR=1,2
      L=(KT-1)*2+KR
      KE=4*(NHEC-1)+L
      U1=0.
      GO TO (71,72,73,74),L
C                                     THETA - THETA
C                                     (TRANSMIT POL. - RECEIVE POL.)
   71 DO 75 J=1,N
      NPJ=N+J
      U1=U1+(RR(J)+ZST(J)*RR(N3+J))*C(J)
      U1=U1+(RR(NPJ)-ZSP(J)*RR(N2+J))*C(NPJ)
   75 CONTINUE
      E(KE)=E(KE)+U1*CSR
      GO TO 16
C                                     THETA - PHI
   72 DO 76 J=1,N
      NPJ=N+J
      U1=U1+(RR(J+N2)-ZST(J)*RR(NPJ))*C(J)
      U1=U1+(RR(N3+J)+ZSP(J)*RR(J))*C(NPJ)
   76 CONTINUE
      E(KE)=E(KE)+U1*SNR
      GO TO 16
C                                     PHI - THETA
   73 DO 77 J=1,N
      NPJ=N+J
      U1=U1+(RR(J)+ZST(J)*RR(N3+J))*C(J)
      U1=U1+(RR(NPJ)-ZSP(J)*RR(N2+J))*C(NPJ)
   77 CONTINUE
      E(KE)=E(KE)+U1*SNR
      GO TO 16
C                                     PHI - PHI
   74 DO 78 J=1,N
      NPJ=N+J
      U1=U1+(RR(J+N2)-ZST(J)*RR(NPJ))*C(J)
      U1=U1+(RR(N3+J)+ZSP(J)*RR(J))*C(NPJ)
   78 CONTINUE
      E(KE)=E(KE)+U1*CSR
   16 CONTINUE
   27 CONTINUE
   58 CONTINUE
   41 CONTINUE
C                                     WRITE OUTPUTS
      DO 28 NHEC=1,3
      DO 29 KT=1,2
```

```
      WRITE(6,18)NHEC,KT
      WRITE(6,19)
      J1=N*(2*NHEC+KT-3)
      DO 37 J=1,N
      J2=J+J1
      TJ(J2)=TJ(J2)*R2(J)
      PJ(J2)=PJ(J2)*R2(J)
      WRITE(6,38)TJ(J2),PJ(J2)
   37 CONTINUE
      WRITE(6,119)
      DO 137 J=1,N
      J2=J+J1
      TM(J2)=-ETA*ZSP(J)*PJ(J2)
      PM(J2)=ETA*ZST(J)*TJ(J2)
      WRITE(6,38)TM(J2),PM(J2)
  137 CONTINUE
      DO 30 KR=1,2
      J1=4*NHEC+2*KT+KR-6
      SIG=P4*E(J1)*CONJG(E(J1))
      WRITE(6,10)NHEC,KT,KR,SIG
   30 CONTINUE
   29 CONTINUE
   28 CONTINUE
      STOP
C                              FORMAT STATEMENTS
C
    9 FORMAT('0SAMPLE OUTPUT FROM SUBROUTINES')
    8 FORMAT(1X,4E14.7)
   18 FORMAT('0NHEC=',I3,', KT=',I3)
   19 FORMAT('   REAL JT    IMAG JT    REAL JP    IMAG JP')
  119 FORMAT('   REAL MT    IMAG MT    REAL MP    IMAG MP')
   38 FORMAT(1X,4E11.4)
   10 FORMAT(' NHEC=',I3,', KT=',I3,', KR=',I3,
     1', SIGMA/(LAMBDA)**2=',E11.4)
   49 FORMAT('  NM NP NPHI'/1X,2I3,I4)
   48 FORMAT(7X,'BK',12X,'TT',13X,'P',12X,'TR',12X,'PR'/1X,
     15E14.7/7X,'ALP'/1X,E14.7)
   45 FORMAT(' RH'/(1X,8F8.4))
   44 FORMAT(' ZH'/(1X,8F8.4))
   47 FORMAT(' X'/(1X,5E14.7))
   43 FORMAT(' A'/(1X,5E14.7))
  100 FORMAT(1X,'  ZS =',2F10.4)
      END
C   SUBROUTINE MATB - THIS ROUTINE CALCULATES THE MATRIX (B)
C      WHICH IS PART OF THE NORMALIZED IMPEDANCE (ADMITTANCE)
C      MATRIX OF THE IBC EFIE (MFIE) WHEN THE SURFACE IMPEDANCE
C      IS NON-ZERO:
C
```

```
C                        (B) (J)  =  1.0/ETA  (N) (A) (N)
C
C      WHERE  (A)  IS A P.C. ADMITTANCE (IMPEDANCE) MATRIX, (N)
C      REPRESENTS THE EXPANSION COEFFICIENTS OF THE MAGNETIC
C      SURFACE CURRENT DENSITY,  (I)  REPRESENTS THOSE OF THE
C      ELECTRIC CURRENT, (N) REPRESENTS THE CROSS PRODUCT OF THE
C      OUTWARD UNIT SURFACE NORMAL AND ETA IS THE FREE SPACE WAVE
C      IMPEDANCE.
C
      SUBROUTINE MATB(N2,ZSP,ZST,X)
      COMPLEX X(1),ZSP(1),ZST(1),CTEMP
      N=N2/2
      N2N=N2*N
C                                   I DENOTES ROW, J DENOTES COLUMN.
C                                   I1, I2, I3 AND I4 ARE IN THE TT,
C                                   PT, TP AND PP SUBMATRICES OF X
C                                   RESPECTIVELY.
        DO 10 J=1,N
        I1=(J-1)*N2+1
        I2=I1+N
        I3=I1+N2N
        I4=I3+N
          DO 20 I=1,N
          CTEMP=X(I4)
          X(I4)=X(I1)*ZSP(J)
          X(I1)=CTEMP*ZST(J)
          CTEMP=X(I3)
          X(I3)=-X(I2)*ZSP(J)
          X(I2)=-CTEMP*ZST(J)
          I1=I1+1
          I2=I2+1
          I3=I3+1
          I4=I4+1
   20     CONTINUE
   10   CONTINUE
      RETURN
      END
```

ACKNOWLEDGMENT

The author would like to acknowledge Gregory E. Heath of the Lincoln Laboratory Radar Signature Studies Group for his help in the integral equation formulation and for numerous helpful suggestions concerning the numerical examples. Also, the author greatly appreciated the excellent typing support of Donna McTague, secretary of the Radar Signature Studies Group.

REFERENCES

1. M. A. Leontovich, "Appendix of Diffraction, Refraction and Reflection of Radio Waves," (thirteen papers by V. A. Fock, N. Logan and P. Blacksmith, eds.), U.S. Gov. Printing Office, Washington, D.C. (1957), DDC AD-117276.

2. V. H. Weston, "Theory of Absorbers in Scattering", IEEE Trans. Antennas Propag. AP-11, 578 (1963).

3. T.B.A. Senior, "Impedance Boundary Conditions for Imperfectly Conducting Surfaces," Appl. Sci. Res., Section B, 8, 418 (1960).

4. J. J. Bowman, "Effects of Absorbers," in Methods of Radar Cross Section Analysis (Academic Press, New York, 1968).

5. K. M. Mitzner, "An Integral Equation Approach to Scattering From a Body of Finite Conductivity," Radio Sci 2, 1459 (1967).

6. F. K. Oshiro, et. al., "Calculation of Radar Cross Section," Part I, Vol. I, Technical Report AFAL-TR-67-308 Wright-Patterson AFB, Ohio (December 1967).

7. F. K. Oshiro, K. M. Mitzner, S. S. Locus, et. al., "Calculation of Radar Cross Section. Part II. Analytical Report," Technical Report AFAL-TR-70-21 Wright-Patterson AFB, Ohio (April 1970), DDC AD-867969.

8. R. D. Graglia and P. L. E. Uslenghi, "Electromagnetic Scattering by Impedance Bodies of Revolution", National Radio Science Meeting, session URSI/B-6-3, paper 4, University of Houston, Houston, Texas, 23-26 May 1983.

9. K. A. Iskander, L. Shafai, A. Frandsen, and J. E. Hansen, "Application of Impedance Boundary Conditions to Numerical Solution of Corrugated Circular Horns," IEEE Trans. Antennas Propag. AP-30, 366 (1982).

10. G. E. Heath, "Well-Posed Formulations of Impedance Boundary Condition Integral Equations," Technical Report Lincoln Laboratory, M.I.T. (To Be Published).

11. J. R. Mautz and R. F. Harrington, "H-Field, E-Field and Combined-Field Solutions for Conducting Bodies of Revolution," Arch. Elect. Ubertragung 32, 157 (1978).

12. _____, "H-Field, E-Field and Combined-Field Solutions for Bodies of Revolution," Technical Report TR-77-2, Department of Electrical and Computer Engineering, Syracuse University, Syracuse, New York (February 1977).

13. _____, "Computer Programs for H-Field, E-Field, and Combined Field Solutions for Bodies of Revolution," Technical Report TR-77-3, Department of Electrical and Computer Engineering, Syracuse University, Syracuse, New York (May 1977).

14. J. R. Wait and C. M. Jackson, "Calculations of the Bistatic Scattering Cross Section of a Sphere With an Impedance Boundary Condition," Radio Sci. J. Res. NBS/USNC-URSI, 69D, 299 (1965).

15. R. F. Harrington, Time Harmonic Electromagnetic Fields (McGraw-Hill, New York, 1961).

16. A. J. Poggio and E. K. Miller, "Integral Equation Solutions of Three-Dimensional Scattering Problems," in Computer Techniques for Electromagnetics, R. Mittra, ed. (Oxford, Pergamon Press, New York, 1973).

17. G. T. Ruck, D. E. Barrick, W. D. Stuart and C. K. Krichbaum, Radar Cross Section Handbook, Volume 2 (Plenum Press, New York, 1970), p 612.

18. R. Mittra and C. A. Klein, "Stability and Convergence of Moment-Method Solutions," in Numerical and Asymptotic Techniques in Electromagnetics, R. Mittra, ed. (Springer-Verlag, New York, 1975), p 129.

19. LINPACK, User's Guide (SIAM, Philadelphia, 1979).

20. G. Strang, Linear Algebra and Its Applications, 2nd Ed. (Academic Press, New York, 1980).

21. D. S. Jones, "Numerical Methods For Antenna Problems", Proc. IEE 121, 573 (1974).

GLOSSARY OF SYMBOLS
(Order of Appearance)

IBC	Impedance boundary condition (Leontovich)
MFIE	IBC magnetic field integral equation
EFIE	IBC electric field integral equation
CFIE	IBC combined field integral equation
BOR	Body of revolution
$\overleftrightarrow{Z}_s$	Dyadic normalized surface impedance (double arrow denotes dyadic)
$(\vec{E}^i, \vec{H}^i)$	Incident electromagnetic fields (arrow denotes vector)
S	Closed surface of imperfectly conducting body
$e^{j\omega t}$	Sinsusoidal time dependance (phasor notation)
$\vec{J}_{vol}$	Volume electric current density
$(\vec{E}^s, \vec{H}^s)$	Scattered electromagnetic fields
$(\vec{J}, \vec{M})$	Equivalent electric ($\vec{J}$) and magnetic ($\vec{M}$) surface current densities
$\hat{n}$	Outward unit normal to surface (symbol over n denotes unit vector)
x	Vector cross product in equations
$(\vec{E}_\pm, \vec{H}_\pm)$	Total electromagnetic fields just outside (+) or just inside (-) equivalent current surface
$\vec{r}$	Field point vector (source point when primed)
η	Free space wave impedance
.	Vector scalar product in equations
$\int_s$	Principal value surface integration
μ	Permeability of medium surrounding body (free space)
Φ	Free space Green's function

GLOSSARY OF SYMBOLS (Cont'd)

∇	Del operator (operates on source point coordinate when primed) used for gradient ($\nabla\phi$), divergence ($\nabla\cdot A$) or curl ($\nabla \times A$)
ε	Permittivity of medium surrounding body
π	Pi = 3.14159...
k	Wavenumber
$\lvert\ \rvert$	Absolute value (length)
$\tilde{Z}_a$	Generalized integral equation weighting coefficient
L_E, L_H	Perfect conductor integro-differential operators
α	Scalar, constant integral equation weighting coefficient
ϕ	Cylindrical surface azimuthal coordinate
t	Surface coordinate along BOR generating curve
f	Triangular expansion function
$\hat{W}$	Moment-method testing function
[ ]	Matrix
[V]	Source from incident electric field vector
[Z]	Normalized impedance matrix for perfect conductor EFIE (not to be confused with surface impedance)
[I]	Electric current expansion coefficients (unknown)
[U]	Source from magnetic field vector
[Y]	Normalized admittance matrix for perfect conductor MFIE
[N]	Matrix representing $\hat{n}$ x vector operation
[M]	Magnetic current expansion coefficients

GLOSSARY OF SYMBOLS (Cont'd)

[ZZ]	Generalized impedance matrix for the IBC EFIE
[YY]	Generalized admittance matrix for the IBC MFIE
$\vec{A}$	Electric vector potential
V	Scalar potential
$\vec{F}$	Magnetic vector potential
(r,θ,ϕ)	Right-handed spherical coordinate system
[R]	Measurement matrix
ρ	Radial cylindrical coordinate
[S]	Generalized measurement matrix
SEG	Moment-method segmentation (segments/wavelength)
Z_s	Scalar, constant normalized surface impedance
ka	Sphere wavenumber - radius product
Re( )	Real part of a complex quantity
Im( )	Imaginary part of a complex quantity
cond	Approximate matrix condition number
σ	Differential scattering cross section
a	Sphere radius
λ	Wavelength
θ	Bistatic scattering angle
ME	Bistatic cross section mean error (percent)

AD-A137 353 NUMERICAL SOLUTIONS TO ILL-POSED AND WELL-POSED IMPEDANCE BOUNDARY CONDIT..(U) MASSACHUSETTS INST OF TECH LEXINGTON LINCOLN LAB J R ROGERS 30 NOV 83 TR-641

2/2

UNCLASSIFIED ESD-TR-83-106 F19628-80-C-0002 F/G 12/1 NL

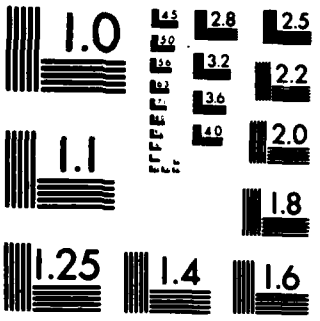

UNCLASSIFIED

SECURITY CLASSIFICATION OF THIS PAGE (When Data Entered)

REPORT DOCUMENTATION PAGE		READ INSTRUCTIONS BEFORE COMPLETING FORM
1. REPORT NUMBER ESD-TR-83-106	2. GOVT ACCESSION NO. AD-A137 353	3. RECIPIENT'S CATALOG NUMBER
4. TITLE (and Subtitle) Numerical Solutions to Ill-Posed and Well-Posed Impedance Boundary Condition Integral Equations		5. TYPE OF REPORT & PERIOD COVERED Technical Report 6. PERFORMING ORG. REPORT NUMBER Technical Report 641
7. AUTHOR(s) James R. Rogers		8. CONTRACT OR GRANT NUMBER(s) F19628-80-C-0002
9. PERFORMING ORGANIZATION NAME AND ADDRESS Lincoln Laboratory, M.I.T. P.O. Box 73 Lexington, MA 02173-0073		10. PROGRAM ELEMENT, PROJECT, TASK AREA & WORK UNIT NUMBERS Program Element Nos. 63304A and 63308A
11. CONTROLLING OFFICE NAME AND ADDRESS Ballistic Missile Defense Program Office Department of the Army 5001 Eisenhower Avenue Alexandria, VA 22333		12. REPORT DATE 30 November 1983 13. NUMBER OF PAGES 98
14. MONITORING AGENCY NAME & ADDRESS (if different from Controlling Office) Electronic Systems Division Hanscom AFB, MA 01731		15. SECURITY CLASS. (of this report) Unclassified 15a. DECLASSIFICATION DOWNGRADING SCHEDULE

16. DISTRIBUTION STATEMENT (of this Report)

Approved for public release; distribution unlimited.

17. DISTRIBUTION STATEMENT (of the abstract entered in Block 20, if different from Report)

18. SUPPLEMENTARY NOTES

None

19. KEY WORDS (Continue on reverse side if necessary and identify by block number)

electromagnetic scattering
integral equation methods
impedance bodies of revolution
impedance boundary condition
numerical solutions

20. ABSTRACT (Continue on reverse side if necessary and identify by block number)

Exterior scattering from impedance bodies is formulated in terms of integral equations derived from the Leontovich impedance boundary condition. Numerical solutions are obtained from the ill-posed electric and magnetic field integral equations and from the well-posed combined field integral equation. Results show that numerical solutions to the ill-posed equations can be severely contaminated by spurious solutions, while those of the well-posed equation are not contaminated when a suitable choice of integral equation weighting coefficient is used.

DD FORM 1 Jan 73 1473 EDITION OF 1 NOV 65 IS OBSOLETE

UNCLASSIFIED

SECURITY CLASSIFICATION OF THIS PAGE (When Data Entered)